



HAL
open science

Comparative analysis of Rayleigh and Love waves detected propagating in the Nobi and Kanto basins during the 2004-, 2007- Chuetsu and 2011 Tohoku earthquakes

Kristel Meza-Fajardo, Hideo Aochi, Apostolos Papageorgiou

► **To cite this version:**

Kristel Meza-Fajardo, Hideo Aochi, Apostolos Papageorgiou. Comparative analysis of Rayleigh and Love waves detected propagating in the Nobi and Kanto basins during the 2004-, 2007- Chuetsu and 2011 Tohoku earthquakes. *Soil Dynamics and Earthquake Engineering*, 2021, 143, pp.106606. 10.1016/j.soildyn.2021.106606 . hal-03747350

HAL Id: hal-03747350

<https://brgm.hal.science/hal-03747350>

Submitted on 22 Mar 2023

HAL is a multi-disciplinary open access archive for the deposit and dissemination of scientific research documents, whether they are published or not. The documents may come from teaching and research institutions in France or abroad, or from public or private research centers.

L'archive ouverte pluridisciplinaire **HAL**, est destinée au dépôt et à la diffusion de documents scientifiques de niveau recherche, publiés ou non, émanant des établissements d'enseignement et de recherche français ou étrangers, des laboratoires publics ou privés.



Distributed under a Creative Commons Attribution - NonCommercial 4.0 International License

Comparative analysis of Rayleigh and Love waves detected propagating in the Nobi and
Kanto Basins during the 2004-, 2007- Chuetsu and 2011 Tohoku earthquakes

By

Kristel C. MEZA FAJARDO^(*), Hideo AOCHI and Apostolos S. PAPAGEORGIU

Submitted to

Soil Dynamics and Earthquake Engineering

(*) Corresponding author

1 ABSTRACT

2 Propagation of long-period ground motion in sedimentary basins has been a subject of great
3 interest among seismologists and engineers. Intense long-period ground motions consist primarily
4 of surface waves that get trapped or generated locally as seismic energy travels through
5 sedimentary deposits. In the present work, we investigate the propagation of surface waves in the
6 basins of Kanto and Nobi in Japan, during three relatively recent events: The Mw 6.6 2004
7 Niigata Chuetsu, the Mw 6.6 2007 Chuetsu-Oki and the Mw 9.0 2011 Tohoku earthquakes. We
8 identify the surface waves using a signal processing technique that detects their polarization
9 characteristics, in the time-frequency space, using orthogonality relations among phase vectors.
10 Then, by applying the “Normalized Inner Product” (NIP), regions of a particular type of
11 polarization are delineated and filters are applied to isolate the associated surface waves, along
12 with their direction of propagation. With our investigation, we attempt to follow the *‘flow’* of
13 seismic energy as it approaches just outside the basins, and then how it evolves once inside the
14 basin. Our analysis shows that the long period (< 0.1 Hz) surface wave energy approaching the
15 Kanto basin during the 2011 Tohoku earthquake consists of Rayleigh waves, and that part of the
16 seismic energy is converted to Love waves. In a higher frequency range (0.1 – 0.5 Hz), prograde
17 Rayleigh and Love waves were detected in selected areas such as the Chiba sub-basin and the
18 Tokyo lowlands. Regarding the Nobi basin, we find that whereas the Rayleigh waves in the
19 frequency range (0.1 – 0.5 Hz) radiated during the 2011 Tohoku earthquake strongly interact with
20 the basin, the Rayleigh waves radiated by the Chuetsu events appear to propagate through the
21 basin unaffected. This difference in basin response is attributed to the different azimuthal
22 direction of incidence of the surface wave energy.

23 Keywords: surface waves, Rayleigh, Love, retrograde, prograde, polarization, wave identification

25 **Introduction**

26 The influence of sedimentary deposits in the form of basins on the intensity of strong
27 ground motion has been recognized by Gutenberg [1] since the middle of the previous century.
28 Starting with the seminal theoretical works of Aki and Larner [2] and Bard and Bouchon [3], [4],
29 and the observational study by King and Tucker [5], great progress has been made in addressing
30 the response of sedimentary valleys to incident seismic waves and the body of published
31 literature on the topic is voluminous. Key earthquake events have provided ample evidence of
32 basin-induced surface waves; among them: the 1967 M_w 6.6 Caracas earthquake [6], the 1985
33 M 8.1 Michoacan earthquake [7], the 1989 M_S 7.1 Loma Prieta earthquake [8], the 1995 M_w 6.9
34 Kobe earthquake [9], the 2001 M 6.8 Nisqually earthquake [10], and the 2003 M_w 8.0, Tokachi-
35 Oki earthquake [11], [12]. The earthquake engineering community is also well aware of basin
36 effects, as recent earthquake events (including the megathrust M_w 9.0 2011 Tohoku earthquake)
37 have exposed the effects of long-period ground motions on large-scale structures, such as high-
38 rise buildings, long-span bridges, fluid-filled tanks, etc. (e.g. [11], [13]).

39 Many studies in Japan focusing on the Kanto and Osaka basin [14]–[20] have observed
40 late-arriving surface waves which have been attributed to a generation process at the edges of the
41 respective sedimentary basins. For basins like Los Angeles basin in California, researchers like
42 Olsen [21], have reported that intense long-period (0 – 0.5 Hz) ground motions can be generated
43 by events located far from the basin edge. Other studies have focused on the effect of the
44 azimuthal angle of long-period seismic waves in basins in Japan [22]–[25]. Surface waves have
45 been also identified via array analysis, in the long period range in microseismic events (e.g.,
46 Seydoux *et al.* [26]), and in the intermediate period range in noise measurements (e.g., Wathelet
47 *et al.* [27]). While most of the published literature recognizes the role of surface waves on the

48 amplification of long period ground motion in sedimentary basins, precise analyses of the
49 propagation of surface waves are difficult to find, in particular analyses from strong ground
50 motion recordings. A few distinctive studies of this kind, early on, are the wave propagation
51 analyses of ground motion recordings in three sedimentary valleys in Central Asia [28], in the
52 Los Angeles basin [29], [30] and in the Mexico Valley [31]. Part of the problem is the fact that
53 surface waves are present in a seismogram along with other types of waves with similar
54 frequencies and arrival times, and their separation has not been a straightforward task.
55 Furthermore, most basins had not been instrumented with seismic networks dense enough as to
56 allow the mapping of the propagation of the different phases. In the last three decades, the
57 nationwide seismic networks (KiK-net, K-NET) in Japan have recorded major, strong events that
58 have generated intense surface waves. These networks have been deployed with a relatively high
59 density, and with instruments capable to record broad-band strong ground motion with high
60 precision.

61 In the present work, we study surface wave propagation from strong ground motion
62 recordings, by exploiting the dense seismological K-NET network, in both the Nobi and Kanto
63 basins. The Nobi basin in Japan is a sediment filled valley extending over an area of about 1800
64 square kilometers. The city of Nagoya, being the fourth-most-populous urban area in Japan with
65 more than 2 million people, is located on the basin. The city has suffered extensive damage
66 during large earthquakes in the past, the 1891 M ~ 8 Nobi earthquake being the most dramatic
67 example [32]. Similarly, the Kanto basin, where Tokyo, the capital of Japan, is located, sustained
68 heavy destruction during the 1923 M ~ 8 Kanto earthquake (e.g. [33]).

69 We analyze the strong ground motion recordings using a recently proposed method
70 (referred to as the Normalized Inner Product method – NIP for short) [34] to identify the various

71 types of surface waves and extract them. We study the propagation of the very complex wave-
72 field that was generated by the megathrust 2011 Tohoku earthquake, and two smaller earthquake
73 events, the 2004 Chuetsu and 2007 Chuetsu-oki events. With [this](#) investigation, we attempt to
74 [track](#) the '*flow*' of seismic energy as it approaches the basin, and inside it. In that effort we try to
75 focus on the composition of the surface wave energy just outside the basin and then inside the
76 basin. We identify the most energetic Rayleigh waves, indicate if they are retrograde or prograde,
77 and provide their direction of propagation. We also identify intense Love waves, extract their
78 waveforms, and estimate their direction of polarization. We establish if the identified seismic
79 energy in the form of surface waves was converted at the basins, or if it arrives to the basins
80 already in the form of surface waves. Our study, among other things, demonstrates the power of
81 the NIP method in analyzing complex wave-fields.

82 This work is organized [in terms of](#) the three earthquake events under study. We first
83 describe the structure of the two basins and briefly present the method of identification of surface
84 waves. Next we compare the surface wave fields generated by the events mentioned above,
85 focusing on the different basin responses. The first event that we present is the Tohoku
86 earthquake, a major event which, due to its large faulting area, radiated to the two basins from a
87 range of azimuthal directions. We then present the Chuetsu and Chuetsu-oki earthquakes
88 together, as these two events have very similar magnitude [and similar](#) mechanism [and their](#)
89 [epicenters are very close to each other](#).

90 **Sedimentary basins**

91 The Nobi basin, located in the central part of Japan (Figure 1a), is a basin with a
92 maximum depth of 3 km composed of Alluvial, Pleistocene and Tertiary strata [35]. On the other
93 hand, the well-known Kanto basin is a deep and geometrically more complex sedimentary basin

94 with an inland bedrock depth as large as 4 km under the Chiba prefecture [36]. The Kanto basin
95 is composed of Quaternary and Tertiary sediments, surrounded on the north and west by
96 mountains composed of volcanic and Pre-Tertiary rocks [16]. Figures 1 and 2 show the bedrock
97 depth of the two basins, indicated by the depth of the layer corresponding to $V_s=2700$ m/s,
98 retrieved from the 3D national deep structure model of the National Research Institute for Earth
99 Science and Disaster Resilience of Japan [37]. According to Figure 2, the Nobi basin can be
100 considered as one concave deposit of soft layers whereas the geometry of the Kanto basin
101 includes deposits in the form of several elongated branches. As the maximum depths of the Nobi
102 and Kanto basins differ significantly **when** compared to each other, we can expect different basin
103 responses to the incoming wave fields. We also note in Figure 2 that, for both Kanto and Nobi,
104 the basin edges are steeper on their western sides.

105 **Earthquake events and recording stations**

106 The source parameters of the three events considered in this study are listed in Table 1,
107 where we note that the Chuetsu and the Chuetsu-oki earthquakes have the same magnitude and
108 similar focal depth. In addition of being closely located, the focal mechanisms for these two
109 earthquakes can be considered virtually identical. Several studies ([Furumura and Hayakawa \[13\]](#),
110 [Yoshimoto and Takemura \[34\]](#)) have already reported the observation of important long period
111 motions associated to these earthquakes. Differing from the Chuetsu and Chuetsu-oki
112 earthquakes by its great size and its location at a subduction zone, the wave field radiated by the
113 Tohoku earthquake allows the observation of different aspects of basin response.

114 In this study we analyze accelerograms of flat broadband response recorded by the K-
115 NET seismographic network [39] at rock outcrop sites and sites within the basins. The spatial
116 distribution of the stations considered in the study is shown in Figures 1b and 1c, although not all

117 stations recorded all three events. We identify and extract Love and Rayleigh waves based on their
 118 characteristic elliptical polarization, which requires that we work with displacement histories.
 119 These displacement histories were derived from the recorded acceleration histories, by band-pass
 120 filtering between 0.05 and 20 Hz with a second order Butterworth filter, and then integrating in
 121 time twice. Figure 3 shows the three components of displacement waveforms at two stations on
 122 rock, station GIF024 in Nobi, and station SIT006 in Kanto, during the three events listed in Table
 123 1. We can observe that the frequency content and duration seem very similar during the two
 124 Chuetsu events. Furthermore, the displacement amplitudes recorded at the two stations, are
 125 comparable (if not the same) for the two events. On the other hand, the amplitudes of the Tohoku
 126 earthquake recordings are an order of magnitude greater, as compared to those of the Chuetsu
 127 events, clearly because of its great size.

128 **Identification and extraction of surface waves**

129 To study the propagation of surface waves, we make use of a signal processing technique
 130 [34] that allows the identification and extraction of wave packets of Rayleigh and Love waves,
 131 along with their direction of maximum energy. In the context of waves trapped in a basin, wave
 132 packets of different frequencies can simultaneously arrive at a station of interest, and thus the
 133 analysis benefits from resolving the signal in the time-frequency domain, by means of the
 134 Stockwell Transform [40]:

$$S(t, f) = \int_{-\infty}^{\infty} h(\tau) \frac{|f|}{\sqrt{2\pi}} \exp\left[-\frac{(t - \tau)^2 f^2}{2}\right] \exp(-2\pi i f \tau) d\tau \quad (1)$$

135 where $h(t)$ is the time-function that is being transformed. Each component of the recorded
 136 motion becomes a complex-valued matrix defined in the discrete time-frequency (t, f) space.
 137 Equivalently, each complex-valued entry of the matrix may be described by a *phasor* (or *phase*

138 *vector*, i.e. a vector defined by the magnitude and the phase/argument of the complex number that
139 it describes; [41]). In Figure 4 we show the amplitudes of the S-transform (i.e. the magnitudes of
140 the phasors) of the vertical components of displacement waveforms presented in Figure 3. We
141 can readily observe in Figure 4 that the dominant frequencies for the two Chuetsu events are in
142 the frequency range 0.1-0.2 Hz, whereas for the large Tohoku earthquake the dominant frequency
143 is below 0.1 Hz. These observations remain consistent for the two stations that are far from each
144 other, one near the Nobi basin and the other near the Kanto basin. Because stations GIF024 and
145 SIT006 are considered to be located on rock, we attribute the observed dominant frequencies to
146 the source characteristics and, possibly, to the propagation path. In particular, the low frequencies
147 (less than 0.1 Hz) observed in the recordings of the Tohoku event, are attributed to the large
148 dimensions of the rupture (e.g. [42]–[44]). However, Figure 4 also shows that the energy radiated
149 by the Tohoku earthquake in the frequency range 0.1-0.5 Hz is still important, and in the sequel,
150 we investigate its interaction with the basins.

151 The basic idea of the method to extract Rayleigh waves, [presented by Meza-Fajardo *et al.*](#)
152 [in \[34\]](#), is to identify regions in the time-frequency space where the particle polarization is
153 elliptical. Because ellipticity is a parameter which rapidly changes in a seismogram, we prefer to
154 identify elliptical polarization by the orthogonality of appropriate phasors of the transformed
155 wave train. We look for regions in the (t, f) space where there is a $\pm(\pi/2)$ phase shift between the
156 phasors of the horizontal and vertical displacement components. This reasoning then leads
157 naturally to the use of the inner product as a tool to identify orthogonality between phasors. The
158 inner product will be zero if the phasors are orthogonal. Furthermore, if the phasors of two
159 components (say the vertical and a horizontal) are orthogonal but one performs a $\pm(\pi/2)$ shift in
160 one of them (say, the phasor of the vertical component of a Rayleigh wave), then the inner

161 product of the two components will be close to 1, if the phasors are normalized by their
162 magnitudes. As shown in [34], the normalized inner product (NIP) of Rayleigh wave components
163 is a parameter that presents less variation with time and frequency as compared to other measures
164 of ellipticity. Then, we can effectively construct filters in the time-frequency (t, f) space to
165 isolate and retain only those regions where the NIP is close to 1 (say $\text{NIP} > 0.8$), and retrieve the
166 waveforms (that is, the time histories) of the desired Rayleigh waves by inverting back to the
167 time domain. The extracted Rayleigh waves are retained only if the correlation coefficient
168 between the time histories of the horizontal and (shifted) vertical component is higher than 0.8.
169 On the other hand, the inner product has proved to be useful **also** in identifying the direction of
170 polarization (or, equivalently of maximum energy) of the horizontal component of a wave train
171 [34], [45], because it can be used to find the two orthogonal horizontal directions for which the
172 correlation is minimum. In the latter case the direction of polarization of Love waves can be also
173 identified. We refer the readers to the previous publications [34], [45] where they can find more
174 details on the wave extraction technique.

175 In the present work, we implement the filtering technique described above at each station
176 independently, and assuming that the surface wave energy dominating the three-component
177 seismogram corresponds to retrograde Rayleigh waves, as it is the mode most commonly
178 observed in ground motion recordings. Prograde Rayleigh waves are also investigated, especially
179 when the direction of retrograde wave propagation among several stations cannot be verified.
180 Finally, waveforms for Love waves are detected independently at each station after both
181 retrograde and prograde Rayleigh waves have been filtered out of the seismogram.

182 **The 2011 Tohoku earthquake**

183 *Surface waves in the lower frequency range (0.05-0.1 Hz)*

184 Figure 5 displays the identified and extracted retrograde Rayleigh waves on both basins in the
185 frequency range 0.05-0.1 Hz. The top panels of Figure 5 illustrate the direction of polarization
186 (this direction is referred to also as the *direction of maximum energy*), and thus, for the case of
187 Rayleigh waves, the direction of propagation, indicated by an arrow at each station where these
188 Rayleigh waves have been identified. The length of each arrow is proportional to the amplitude
189 of the Rayleigh waveform identified at the corresponding station shown in the figure. On the
190 bottom panels, the time histories of selected stations are plotted, showing the two components of
191 Rayleigh waves, the horizontal component in the indicated direction of maximum energy, and the
192 vertical component with a ($\pi/2$) shift. These two components should be in phase - as they appear
193 to be in the figure - if the extracted waves have elliptical polarization, that is, if indeed they are
194 Rayleigh waves. The intermittent straight line, on the top panels indicates the direction of
195 maximum energy averaged over all stations shown in the figure. The wave-traces shown on the
196 bottom panels correspond to stations that were selected by their close proximity to the
197 intermittent straight line that indicates the average direction of propagation. Furthermore, the
198 separation distances of the wave-traces along the vertical dimension of the bottom panels of
199 Figure 5, are proportional to the separation distances between the projections of the positions of
200 the stations on the intermittent straight line. The waveform plot constructed in this fashion
201 permits us to verify visually the direction of polarization (i.e. direction of maximum energy) of
202 the extracted wave. In the case of Rayleigh waves the direction of polarization coincides with the
203 direction of propagation, and thus the waveform plot should show how the waves propagate in
204 the estimated average direction. For the extracted retrograde Rayleigh waves shown in Figure 5,
205 we can assert that this is, in fact, the case.

206 For the Rayleigh waves in the Kanto basin of Figure 5a the average direction of
207 propagation has an azimuth of 245 degrees. The consistent direction of propagation from station
208 to station (Figure 5a, top panel) and the very coherent waveforms (Figure 5a, bottom panel)
209 provides convincing evidence of the passage of the long-period (0.05 – 0.1 Hz) Rayleigh wave
210 phase. Deviations from the average direction of propagation may be attributed to lateral
211 variations of the velocity profile of the medium. On the other hand, the Rayleigh waves of Figure
212 5a in the Kanto basin interact with the northern edge of the basin. Specifically, the incident
213 surface wave energy is diffracted by the edge that is separating the two linear branches of the
214 basin at the north. As a result of this diffraction, part of the incident seismic energy is
215 ‘channelled’ along the north-western linear branch of the basin. [Parenthetically we note that
216 such ‘channeling effects’ have been reported by Miyake & Koketsu [46], for basins in Japan, and
217 by Olsen *et al.* [47], for basins in California.] We also identify retrograde Rayleigh waves in the
218 Kanto basin that propagate to the southeast, with an average azimuth of 158 degrees, as shown in
219 Figure 5b. This particular phase is interpreted as being seismic energy diffracted from the steep
220 north-eastern edge of the basin (indicated by the thick solid line in Figure 5b). Figure 5b displays
221 the presence of these waves only at some stations on the southeast quadrant of the basin (around
222 the Chiba area). We also note that there is an amplification of these diffracted waves at the
223 stations located on the deepest part of the Chiba area (for example, stations CHB013 and
224 CHB016).

225 Figure 6 displays a very different basin response for the extracted retrograde Rayleigh
226 waves propagating in the Nobi basin. The amplitudes of the extracted Rayleigh waves in the
227 Kanto basin are higher (~13 cm) than the amplitudes of the corresponding extracted waves in the
228 Nobi basin (~5 cm); an expected result given that the Nobi basin is farther from the Tohoku

229 rupturing fault. Furthermore, we note in Figure 6 that as the retrograde Rayleigh waves propagate
230 through the Nobi basin, their amplitude, coherence, and direction of propagation is only slightly
231 affected. In contrast to the diffraction phenomena observed in the Kanto basin, we find that
232 because of their long wavelength (relative to the basin depth), the identified Rayleigh waves do
233 not interact with the Nobi basin.

234 Focusing in the Chiba area and working always in the lower frequency band (0.05 – 0.1
235 Hz), we find in the recorded motions the presence of *Love waves* of significant amplitude, as
236 shown in Figure 7. The arrows without head on the left panel of Figure 7 indicate the direction of
237 linear polarization of the extracted waves. Keeping in mind that the direction of propagation of
238 the Love waves is expected to be normal to their direction of linear polarization, we estimate an
239 average direction of propagation of 215 degrees, not very different from the direction of
240 propagation of the Rayleigh waves of Figure 5a (on the western part of the Chiba area). However,
241 the direction is quite different from the direction of propagation of the Rayleigh waves of Figure
242 5b observed on the eastern part of the Chiba area. These results indicate that 0.05-0.1 Hz
243 Rayleigh waves arriving to the Kanto basin are not only being diffracted at its northern edge, but
244 also they are being converted to Love waves in the Chiba area. We also note that the identified
245 Love waves are detected mainly in the deepest parts of the basin, having significantly reduced
246 amplitudes when they reach the Chiba sub-basin edges. Along with the diffracted Rayleigh waves
247 identified earlier for the Chiba area (Figure 5b), we can consider them as *basin-generated* surface
248 waves.

249 Surface waves in the higher frequency range (0.1-0.5 Hz)

250 Figure 8 and 9 display the Rayleigh waves identified in the range 0.1-0.5 Hz propagating through
251 the Kanto and the Nobi basin, respectively. The figures were composed following the same

252 procedure used in Figure 5. The identified waves are not as strong as the corresponding waves in
253 the range of 0.05-0.1 Hz, but being associated with higher frequencies and having amplitudes
254 beyond 6 cm they can potentially have a detrimental effect on engineering structures (e.g., Meza-
255 Fajardo and Papageorgiou [48]). For this higher frequency range, it is clear from Figure 8 and
256 Figure 9 that the incident seismic wave-field interacts strongly with the two basins, as the
257 direction of propagating of the extracted waves varies significantly among stations, and the
258 coherency is rapidly lost as the waves propagate. Furthermore, in the case of the Kanto basin we
259 identify both retrograde and *prograde* Rayleigh waves, shown in Figures 8a and 8b respectively.
260 This finding is illustrated in Figure 10, where we plot the particle motion in the vertical plane
261 oriented in the direction of propagation at stations SIT001 and CHB006. Figure 10a clearly
262 shows that the first Rayleigh wave train identified at station SIT001 (between 120-140 s) is
263 retrograde, as the sense of rotation is opposite to the direction of propagation (given by the
264 positive sense of R; R denotes direction of maximum energy or direction of propagation). For
265 station CHB006 (Figure 10b) we selected the second wave train (between 130-150 s) because its
266 low frequency allows for a clearer drawing of the ellipse, and a prograde particle motion is
267 indeed observed.

268 In Figure 8a we observe multiple wave trains of retrograde Rayleigh waves at most selected
269 stations. These wave trains are responsible for the long duration of the motion in the basin. By
270 looking at the size of the arrows, which is proportional to the amplitude of the extracted waves,
271 we observe that the strongest waves are identified in the deepest parts of the Chiba and Gunma-
272 Saitama areas. As expected, the identified Rayleigh waves arrive with strong intensity from the
273 east, and as they leave the basin on the western edge, they are significantly less energetic, due to
274 the strong interaction with the Kanto basin. In the case of the prograde waves (Figure 8b), the

275 strongest wavetrains are found in the Chiba and the Tokyo bay area. When compared to the
276 retrograde Rayleigh waves, we note that these prograde waves arrive at the stations at relatively
277 later times, which suggests that they are a very localized basin effect. This observation is
278 reinforced by the fact that in Figure 8b prograde waves are identified only within the basin and
279 only in its eastern part. Then, it is reasonable to conclude that the prograde waves, identified both
280 in the Tokyo bay area and in the Chiba area, are *basin-generated* Rayleigh waves and they are in
281 the frequency range of 0.15-0.2 Hz (that is, 5-6.7 s). These results are consistent with those of
282 [Boué et al.](#) [49], who had already pointed out a prograde mode between 4.7 and 7.6 s for the
283 Kanto basin from analyses of ambient seismic fields. In passing we mention that [Tanimoto and](#)
284 [Rivera](#) [50], on the basis of theoretical analysis, attribute prograde Rayleigh wave particle motion
285 to the existence of very slow (i.e. soft) deposits on top of very thick sediments.

286 A different response is observed with the retrograde Rayleigh waves identified in the Nobi
287 basin, shown in Figure 9. A coherent pulse with central frequency of 0.15 Hz is identified at the
288 borders of the basin at stations GIF024 and AIC009, but as the energy reaches the deeper parts of
289 the basin, the pulse is no longer distinguishable. On the other hand, we observe an elongated
290 duration of the Rayleigh waves at station AIC011 which is located in a deeper part of the basin.
291 The longer duration is a consequence of seismic energy being trapped in the basin. This energy,
292 in the form of surface waves, traverses the basin more than once, after being reflected at the
293 edges of the basin. An interesting observation regarding Figure 9 is that although the overall
294 direction of propagation in this higher frequency range (0.1 – 0.5 Hz) is westward, the seismic
295 energy, when it reaches the western, steeper edge of the basin, is partially reflected, while most of
296 the seismic energy is diffracted to the south (this is clearly evident in the record MIE009). The
297 latter phenomenon is reminiscent of a similar diffraction of the incident seismic energy caused by

298 the Hachioji line at the western edge of the Kanto basin, reported for Love waves by [Kinoshita et](#)
299 [al. \[15\]](#), and [Koketsu and Kikuchi \[49\]](#).

300 In Figure 11 we present the extracted Love waves in the Kanto basin in the range 0.1-0.5 Hz.
301 The intermittent line in the map indicates an estimate of the direction of propagation of the Love
302 waves considering it should be normal to the direction of polarization. We observe in Figure 9
303 that the direction of propagation of the Love waves is to the south-west, clearly different from the
304 direction of propagation of the Rayleigh waves in the same frequency range (Figures 8a and 8b).
305 However, the direction of propagation of these Love waves (Figure 11) remains very close to the
306 direction of propagation of the lower frequency (0.05-0.1 Hz) Love waves of Figure 7. We also
307 note that for both frequency ranges, most Love waves are polarized in a direction *parallel to the*
308 *northern edge of the Kanto basin*. The amplitudes of these waves are remarkably higher as they
309 are more than two times the amplitude of the Rayleigh waves identified in the same frequency
310 range. With an amplitude of 15 cm and with a central frequency of 0.14 Hz these waves can
311 subject high-rise buildings and long-period structures to potentially destructive torsional
312 excitation (e.g., [Cao et al. \[52\]](#)). Furthermore, Figure 11 clearly shows that the southern part of
313 the Kanagawa area is not much affected by these Love waves, and it is the Tokyo bay and
314 northwestern Chiba areas where they are much stronger. The amplitudes of these Love waves
315 appear significantly reduced in the southern stations of the Chiba area, and they are negligible
316 outside the basin, [suggesting that these waves too are basin-generated surface waves](#).

317

318 Quantitative characterization of surface waves in the Kanto basin

319 In this section we proceed to quantify basin effects by analyzing the surface waves
320 previously identified, focusing on the waves that we have characterized as ‘basin-generated’. We
321 consider only the basin-generated waves in the frequency range (0.1-0.5 Hz), since basin effects
322 at lower frequencies are not relevant for engineering structures. We quantify the surface waves
323 under investigation using two parameters: (1) central frequency f_o , which is defined as the
324 frequency associated with the maximum amplitude of the S-Transform of the extracted waves;
325 and (2) amplification coefficient A .

326 Typically, the definition of amplification necessitates the use of a reference station on
327 rock. However, in the present case, this is not possible as ‘basin-generated’ waves exist only in
328 the sediments of the basin and do not exist on rock. We proceed to estimate amplification of the
329 prograde Rayleigh and the Love waves extracted at the Kanto basin in the frequency range (0.1-
330 0.5 Hz) by considering two different definitions of the coefficient of amplification A . One way to
331 quantify amplification is by using the amplification coefficient A_1 defined as follows:

$$A_1 = \frac{\max_t |S_O(t, (f_o)_O)| \cdot (f_o)_R}{\max_t |S_R(t, (f_o)_R)| \cdot (f_o)_O} \quad (2)$$

332 where $S_O(t, f)$ is the Stockwell Transform of the extracted waves at a station of ‘observation’,
333 and $S_R(t, f)$ is the Stockwell Transform of the extracted waves at a ‘reference’ station. By
334 necessity, both stations are located inside the basin. Frequencies $(f_o)_O$ and $(f_o)_R$ are the central
335 frequencies of the extracted waves at the station of ‘observation’ and the ‘reference’ station,
336 respectively. The ratio of Eq. (2) then takes into account the fact that we are comparing wave
337 amplitudes of different frequencies, a necessary consideration when analyzing dispersive wave
338 packets [53]. Furthermore, to minimize interference with other type of surface waves (Love

339 waves for example), we use the vertical component to measure the amplification coefficient of
340 the Rayleigh waves. As 'reference station', we select a station that is at the beginning of the
341 wave-path of the basin-generated waves, where these particular waves are at their inception. In
342 Figure 12a we show the spatial distribution of the central frequency of the identified prograde
343 Rayleigh waves, and in Figure 12b the corresponding amplification coefficient A_1 . Based on
344 Figure 8b, we selected station CHB005 as the reference station. For a better illustration of the
345 results, in Figure 12a we size the circles according to the amplification coefficient shown in
346 Figure 12b. Figure 12 illustrates not only that the prograde Rayleigh waves are stronger at the
347 northern edge and on the Chiba sub-basin, but also the dominant frequency associated with these
348 waves decreases as they reach the southern edge of the basin. Evidently, depth of the sediments
349 appears to be the controlling factor of the central frequency of these waves.

350 Figure 13 displays the central frequency and amplification coefficient of the extracted Love
351 waves. Based on Figure 11, we selected station IBR012 as the reference station, at which the
352 extracted waves have a central frequency of 0.46 Hz. To estimate the amplification coefficient for
353 Love waves we use the horizontal component in the direction of polarization (direction of
354 maximum energy) shown in Figure 11. First, we observe that the central frequency of the Love
355 waves is in most stations lower than that of the prograde Rayleigh waves. Figure 13 also displays
356 that the spatial distributions of the amplification coefficients, associated with Love and prograde
357 Rayleigh waves, differ significantly. The strongest amplification of Love waves is concentrated
358 more in the Tokyo bay area and along the northern part of the Chiba sub-basin. Let us note that
359 the generation of Love waves during the Tohoku earthquake in this frequency range was
360 remarkable, having reached values of amplification coefficient A_1 as high as 35.

361 However, amplification as defined by coefficient A_1 (Eq. 2), is associated with two
362 weaknesses: (1) Selection of the reference station is subjective and, depending on the distribution
363 of stations, may not always be feasible; (2) being associated with the ratio of spectral amplitudes
364 at two specific frequencies, the value of the ratio is expected to be very sensitive and,
365 accordingly, it may vary significantly over a wide range. Stating this differently, one would need
366 a very large number of recordings to obtain statistically significant, and therefore useful, average
367 estimates of amplification. To circumvent both difficulties, we propose an alternative definition
368 for the coefficient of amplification; we refer to this alternative definition of amplification
369 coefficient as A_2 . Specifically, based on the definition of the Stockwell transform, it is evident
370 that $|S(t, f)|^2$ is proportional to an estimate $\hat{G}_{xx}(t, \omega)$ of the (one-sided) evolutionary Power
371 Spectral Density (PSD) function of the stochastic process, a realization of which is the signal
372 (strong motion recording) under analysis [54], [55]. Specifically, $\hat{G}_{xx}(t, 2\pi f) =$
373 $(2\sqrt{\pi}/f)|S(t, f)|^2$. We proceed to define a ‘frequency function’ $\mathbb{S}_E(f)$ (which is a measure of
374 the energy of the signal at frequency f) and its average value \mathbb{S}_E^{av} for the range of frequencies
375 $f_\ell < f < f_h$ over which the energy of the signal is distributed :

$$\mathbb{S}_E(f) = \int_0^\infty \frac{|S(t, f)|^2}{f} dt \quad \mathbb{S}_E^{av} = \frac{1}{(f_h - f_\ell)} \int_{f_\ell}^{f_h} \mathbb{S}_E(f) df \quad (3)$$

376 The frequencies f_ℓ and f_h are selected so that $\int_0^{f_\ell} \mathbb{S}_E(f) df / \int_0^{+\infty} \mathbb{S}_E(f) df = 0.005$ and
377 $\int_0^{f_h} \mathbb{S}_E(f) df / \int_0^{+\infty} \mathbb{S}_E(f) df = 0.995$. This approach is adopted to avoid frequency ranges at
378 the margins, over which the energy is practically zero, which biases the value of \mathbb{S}_E^{av} . Based on
379 the above considerations, we define the alternative amplification coefficient A_2 as follows :

$$A_2 = \sqrt{\frac{S_{E_TOTAL}^{av}}{S_{E_BODY}^{av}}} \quad (4)$$

380 where $S_{E_TOTAL}^{av}$ is associated with the *total* signal (i.e. all phases / types of waves are included),
 381 while $S_{E_BODY}^{av}$ is associated with the signal after surface waves have been extracted and only
 382 body waves remain in the signal. It should be pointed out that A_2 appears to be a stable measure
 383 of amplification, unlike A_1 which is sensitive to the choice of a reference station and to the
 384 specific frequencies involved in its definition. Evidently, if there are no extracted surface waves
 385 in the strong motion record, then $A_2 = 1$. It must be pointed out that A_2 measures the
 386 amplification of surface waves relative to the body waves of the same station which themselves
 387 may undergo a measure of amplification due to the presence of the sediments.

388 Figures 12a and 13a display the central frequency f_o and the amplification coefficient A_1 of
 389 prograde Rayleigh and Love waves, respectively. The central frequency f_o appears to be
 390 controlled by the depth of the sediments for both types of surface waves (Figures 12a and 13a).
 391 Regarding the amplification coefficient A_1 , the picture appears to be rather clear for Love
 392 waves (Figure 13b): A_1 appears to increase with the depth of the sediments, as one moves away
 393 from the northern edge of the Chiba sub-basin which apparently was the diffractor that generated
 394 these waves. Turning our attention to the amplification of the prograde Rayleigh waves, as
 395 measured by the coefficient A_1 (Figure 12b), the results indicate that the highest amplifications
 396 are registered in the vicinity of the deepest parts of the Chiba sub-basin.

397 Considering now the amplification coefficient A_2 , shown in Figures 14b and 14d, we observe
 398 that the values A_2 obtained are much lower than the corresponding coefficients A_1 . Let us recall
 399 that A_2 has a different meaning than A_1 , since it measures how much the surface waves increase
 400 the body wave energy in a frequency range at a station. Therefore, it is not surprising that the two

401 coefficients A_1 and A_2 give different results, and the choice between the two should be based on
 402 the analyst's objectives. However, we note that for both coefficients A_1 and A_2 , the amplification
 403 of Love waves is consistently higher as compared to amplification of Rayleigh waves.
 404 Furthermore, for both A_1 and A_2 , the amplification of Love waves (Figure 14d) is strong in the
 405 neighborhood of the northern edge of the Chiba sub-basin while it is lower everywhere in the
 406 southern part of the area. On the other hand, for prograde Rayleigh waves the values of A_2 do not
 407 exceed 1.5 and the highest values are in the area of the northern edge of the Chiba sub-basin
 408 (Figure 14b). The spatial distributions of the amplification coefficients A_1 and A_2 are very
 409 different, since the highest values of A_1 are located in the deepest part of the Chiba sub-basin
 410 (Figure 12b), mainly in part due to the very low central frequencies identified in that region.

411 Another parameter that may be computed from energy estimations via de S-transform is the
 412 relative group delay time t_{dr} , which is defined as the time delay of arrival of the maximum
 413 amplitude of the S-Transform of the extracted wave relative to the time of arrival of a reference
 414 frequency f_r :

$$t_{dr} = \frac{\int_0^{\infty} t \cdot |S_{SW}(t, f_o)|^2 dt}{\int_0^{\infty} |S_{SW}(t, f_o)|^2 dt} - \frac{\int_0^{\infty} t \cdot |S_{BODY}(t, f_r)|^2 dt}{\int_0^{\infty} |S_{BODY}(t, f_r)|^2 dt} \quad (5)$$

415 Since in the recordings we observe basin effects at frequencies below 1 Hz, we select 2 Hz as
 416 the reference frequency f_r . We associate this reference frequency f_r to body waves, regarding
 417 possible dispersion effects for these waves as not significant. On the other hand, surface waves
 418 are known for propagating as highly dispersive wave packets and usually having a late arrival
 419 time, elongating the duration of the signal, and thus the relative time delay is a parameter of
 420 interest to quantify surface waves. Eq. (5) (above) makes feasible the automation of the process
 421 of t_{dr} determination. Figures 14a and 14c display the relative group delay time t_{dr} of the

422 prograde Rayleigh and Love waves, respectively, in the 0.1-0.5 Hz frequency range. We observe
423 that the relative time delay of Love waves is more organized in space compared to that of the
424 prograde Rayleigh waves. For both prograde Rayleigh and Love waves, we observe that the
425 maximum values of t_{dr} are similar and that they are located in the Tokyo lowlands, finding also
426 high values of t_{dr} at the Chiba sub-basin. Those are the regions where the identified surface
427 waves (especially Love waves) have very low central frequencies, suggesting that the dispersion
428 of surface waves is highly influenced by the local geological structure.

429

430 **The Chuetsu and Chuetsu-oki earthquakes**

431 Surface waves in the frequency range (0.1-0.5 Hz)

432 We perform a similar surface wave analysis for the Chuetsu and Chuetsu-oki events, but now we
433 focus only in the frequency range 0.1-0.5 Hz, as this is the frequency range we identified in
434 Figure 4 for these two events. Also, due to space limitations we only estimate the central
435 frequency of the extracted waves and the amplification coefficient A_1 . In Figures 15 and 16 we
436 present the waveforms and direction of propagation of the retrograde Rayleigh waves identified
437 on the recordings of the basins. We start again with the Nobi basin (Figures 15a and 15b), which
438 is receiving seismic radiation by these two events from the northeast. Retrograde waves with the
439 same central frequency (0.13-0.15 Hz) arrive to the Nobi basin during both Chuetsu earthquakes,
440 the Rayleigh waves from the Chuetsu-oki event being more energetic. From Figure 15 we make
441 the following observations: (i) there is little loss of coherency among stations located at very
442 different points on the Nobi basin, (ii) the direction of propagation of the extracted waves is
443 similar among stations, and (iii) amplification is present only at stations MIE003, located over the
444 deepest part of the basin. The extracted Rayleigh waves identified previously (Figure 9) for the

445 Tohoku earthquake have similar central frequency, but apparently the incident seismic field has a
446 broader frequency content, as compared to the almost monochromatic incident wave-field of the
447 two Chuetsu events (Figures 15a, b). Furthermore, the Nobi basin receives radiation from both
448 Chuetsu events over a very narrow range of azimuthal angle (practically from one azimuthal
449 angle) while in the case of the Tohoku event the basin receives radiation over a wider range of
450 azimuthal angles, due to the very large size of the Tohoku source.

451 In the Kanto basin we observe that the propagation of retrograde Rayleigh waves is [again](#)
452 similar for the two Chuetsu earthquakes (Figures 16a and 16b). A Rayleigh wave train of shorter
453 duration (relative to that of Nobi), propagates with an average azimuthal direction close to 120
454 degrees, and is amplified at stations GNM008 and GNM010. We observe same amplitudes and
455 frequencies at several stations that recorded the two events, for example, stations GNM010 and
456 CHB005. After leaving the narrow channel-type structure the wave train is reduced in coherency
457 and amplitude, as it is scattered and ‘diffused’ within the basin. A coherent wave train can be
458 identified (for both events) traveling south along the edge of the basin, osculating the [western](#)
459 [edge of the basin](#) and, interestingly, no retrograde Rayleigh waves are detected in the deepest
460 parts of the Kanto basin. [The phases observed on stations IBR014 and CHB005 for the Chuetsu](#)
461 [earthquake, and on stations CHB004 and CHB005 for the Chuetsu-oki earthquake, may be](#)
462 [dispersed \(and possibly diffracted\) versions of the corresponding phases observed earlier in the](#)
463 [narrow channel-type structure.](#)

464 In Figures 17(a) and (b) we present the prograde Rayleigh waves identified at the Kanto
465 basin during the two Chuetsu events. Considering the randomness inherent to all seismic events,
466 there is a striking similarity among the waveforms and the spatial distribution [of](#) the stations
467 where prograde waves were identified during the two events. The waveforms identified on the

468 recordings of stations located in the Tokyo bay area have strong amplitudes [as indicated by the
469 arrows in Figures 17(a) and (b)], and they also have a significantly longer duration, relative to the
470 retrograde waves. Let us note that numerous long-period high-rise buildings are located in the
471 Tokyo bay area, which can be significantly affected by these waves having central frequencies in
472 the range 0.12-0.16 Hz. During the Tohoku earthquake the prograde waves in the Tokyo bay area
473 propagate along an East-West direction (see Figure 8b), whereas for the Chuetsu events they
474 propagate along an average azimuthal direction close to 150 degrees, which suggests that these
475 prograde waves propagate in the Tokyo bay area without a preferred direction related to the basin
476 structure. Finally, the maps in Figures 17(a) and (b) show how these prograde waves become
477 weaker and diffracted as they approach the southeastern border of the basin.

478 Next, we turn our attention to the Love waves identified in the Kanto basin during the
479 Chuetsu events, the time histories of which are displayed in Figures 18(a) and (b). We observe
480 that the most energetic Love waves are present in the Saitama-Tokyo area, including the Tokyo
481 bay area. In the Chiba area the amplitude of the Love waves is considerably smaller, even though
482 the basin reaches its maximum depth in this area, illustrating once more the importance of the
483 azimuthal direction of the energy arriving at the basin. It is worth pointing out that once again the
484 Love waves identified near the northern edge of the basin are polarized in a direction parallel to
485 that edge. The waves identified close to the western edge (which is oriented along a north-south
486 direction) of the Kanto basin are also polarized in a direction parallel to the edge. That Love
487 waves can be generated by the north-western edge of the Kanto basin has been suggested by
488 [Kinoshita et al. \[15\]](#), based on observations from previous events arriving from the southwest.
489 Furthermore, this ‘behavior’ of Love waves polarized parallel to the edge of a basin has been
490 already observed in other basins, like Los Angeles basin [56].

491 *Amplification of surface waves in the Kanto basin*

492 In the previous section, we illustrated how the two (very similar) Chuetsu events
493 reproduced very closely the propagation of the [simple](#) Rayleigh retrograde [wave-train](#) arriving to
494 [the Kanto Basin](#) from the northwest, along with the generation of Love and prograde Rayleigh
495 waves. The similarity is more evident when we map the central frequencies and amplification
496 factors of the extracted waves. In Figures 19 and 20 we present the quantification of these
497 parameters for the waves that we consider ‘basin-generated’ (the prograde Rayleigh and Love
498 waves). Stations GNM010 and GNM013 were selected as reference stations for Love and
499 prograde Rayleigh waves, respectively. Note that even though station GNM009 is at the
500 beginning of the wave path as displayed in Figure 18, we cannot use it as reference station since
501 there are no identified Love waves in the recordings. Both figures depict the very similar spatial
502 distribution of central frequencies and amplification coefficients during the two Chuetsu
503 earthquakes. In the areas of Tokyo and Chiba, the central frequency of prograde Rayleigh waves
504 is in the range 0.15-0.2 Hz, whereas for Love waves it is in the lower range 0.1-0.15 Hz. From
505 numerical simulations [Kato et al.](#) [16] had already identified Love waves of 0.125 Hz
506 propagating in Tokyo. It is important to point out that the coefficient of amplification for Love
507 waves is associated with higher values for this lower central frequency. Juxtaposed to the
508 response to the Tohoku event and [being](#) different from it, the spatial distribution of high
509 amplification of the prograde Rayleigh waves during the Chuetsu events is concentrated in the
510 Tokyo and Chiba areas, far from the edges. For Love waves we find *a very similar* spatial
511 distribution of the central frequencies during the Tohoku and two Chuetsu earthquakes (compare
512 Figures 13 and 20), suggesting that the central frequency of Love waves is strongly dependant on
513 the local geological structure. During the two Chuetsu events, we observe important

514 amplification on the stations next to the western edge, related to the generation of Love waves by
515 that edge. Another similarity regarding Love waves induced in the basin by the three events is
516 that the amplification coefficient in the southern Chiba area is not as strong as in the Tokyo and
517 Saitama areas. The peak values of Love-wave amplification are observed in the vicinity of the
518 Tokyo bay area. However, amplification during the Tohoku earthquake was three times larger
519 than the amplification during the Chuetsu events, indicating that earthquake magnitude and
520 azimuthal angle of the incident seismic energy [may](#) have a strong effect on the amplitude of Love
521 waves.

522 **Conclusions**

523 We have identified and analyzed surface waves in the Nobi and Kanto basins in Japan, recorded
524 during the Tohoku, Chuetsu and Chuetsu-oki earthquakes. We have extracted the waveforms of
525 the different types of [surface](#) waves (retrograde Rayleigh, prograde Rayleigh and Love waves)
526 and we have quantified their direction of polarization/propagation. We consider three earthquake
527 events which allow us to perform comparisons among (a) a very large and two smaller events
528 exciting the basins from different azimuths, and (b) two events ('twin' events) having close
529 epicentral location and similar focal mechanisms. In order to quantify basin effects we measure
530 the central frequency of the extracted waves and we estimate an amplification coefficient, giving
531 for the first time a measure of amplification of extracted surface waves. [We also present](#)
532 [preliminary results of the relative group delay time \$t_{dr}\$ of the basin generated surface waves](#)
533 [\(Love waves and prograde Rayleigh waves in the frequency range 0.1 – 0,5 Hz\) in the Kanto](#)
534 [basin during the 2011 Tohoku earthquake.](#) We can summarize the findings of our study as
535 follows:

536 - Low frequency (<0.1 Hz) seismic energy, in the form of retrograde Rayleigh waves arriving at
537 Nobi during the Tohoku earthquake, does not interact with the basin. On the other hand, the
538 higher frequency (0.1-0.5 Hz) Rayleigh waves incident on the basin, interact with the Nobi basin,
539 being diffracted and amplified by it. The latter observation is in contrast to the fact that the (0.1-
540 0.5 Hz) Rayleigh waves, arriving at Nobi during the two Chuetsu earthquakes, do not interact
541 with the basin. We attribute this difference in response to the fact that for the Chuetsu events the
542 azimuthal direction of incidence is very narrow as compared to that during the Tohoku
543 earthquake. In the latter event, due to its great size, radiation is arriving at the Nobi basin over a
544 considerably wider azimuthal range. Some of the azimuthal angles of the latter range may favor
545 interaction of the basin with the incident Rayleigh waves in the frequency range 0.1-0.5 Hz.

546 - Seismic energy radiated by the Tohoku event, in the low frequency range (<0.1 Hz), consisting
547 of retrograde Rayleigh waves was diffracted by the Kanto basin. One of the consequences of that
548 diffraction was the generation of Love waves. The Kanto basin is deeper and considerably
549 larger/wider as compared to the Nobi basin. This fact, along with the smooth velocity gradients
550 with depth of the sediments, may have favored strong excitation of Love waves in the Kanto
551 basin, [as suggested also by Yoshimoto and Takemura \[38\], \[57\]](#).

552 - Prograde Rayleigh waves and Love waves are observed in the Kanto basin (Tokyo lowlands and
553 the Chiba area) in the [frequency](#) range 0.1-0.5 Hz. Conditions favoring the generation of prograde
554 Rayleigh waves include the existence of very soft layers overlying very deep sediments. These
555 conditions apparently exist in the Tokyo lowlands and the deeper parts of the Chiba sub-basin.

556 - It is important to note that Love waves (0.1-0.5 Hz) in the Kanto basin can reach as high as
557 twice the amplitude of the Rayleigh waves in the same frequency range. This has important

558 implications for the torsional response of high-rise buildings and should be an important
559 consideration in the design process of such important structures.

560 -The spatial distribution of the central frequency of the extracted Love waves was very similar for
561 the three events, linking this central frequency to the local basin structure. Also, for all three
562 events, the observed central frequencies of the Rayleigh waves were higher than those of the
563 Love waves.

564 - For the three events, the peak values of Love wave amplification, were located in the vicinity of
565 the Tokyo bay area, and are probably related to the saturation of the lowlands. However,
566 amplification of Love waves during the Tohoku earthquake reached values three times higher
567 than the peak values of amplification during the Chuetsu events. This indicates that amplification
568 [may be](#) affected by the azimuthal direction of incidence.

569 - Both Chuetsu events (being ‘twin’ events as having the same magnitude and the same
570 mechanism) generated very similar Rayleigh and Love waves, and very similar spatial
571 distribution of amplification. This observation suggests that although the generation and
572 propagation of seismic waves involve many uncertainties, key physical features of their
573 generation and propagation are repeatable, and therefore can be modeled and predicted. It should
574 be pointed out though that, as [Mukai et al. \[58\]](#) and [Uetake \[59\]](#) have demonstrated, factors such
575 as the heterogeneous subsurface structure may affect, on occasion significantly, the seismic
576 excitation and response of sedimentary basins. However, it is imperative that more events are
577 analysed in order to identify patterns of generation/amplification of surface waves in sedimentary
578 basins, so as [to identify the factors that control their generation and intensity and, eventually, to](#)
579 [develop](#) the capability to predict them and synthesize them with confidence.

580 **Data and Resources**

581 All seismograms used in this work were recorded at K-NET stations, made available by the
582 National Research Institute for Earth Science and Disaster Prevention (NIED) on their website
583 (<http://www.kyoshin.bosai.go.jp/>, last accessed October 2019). The earthquake information was
584 also provided by NIED (<http://www.fnet.bosai.go.jp/>, last accessed October 2019). The 3D
585 models of bedrock depth for the Nobi and Kanto basins were retrieved from the 3D national deep
586 structure model of NIED (<http://www.j-shis.bosai.go.jp/>, last accessed October 2019).

587 The relief geographic map of Japan in Figure 1 was generated with the code READHGT written
588 by François Beauducel, from the Institute de Physique du Globe de Paris.

589 **Acknowledgements**

590 The authors are grateful for the comments of three anonymous reviewers that improved the
591 clarity of the manuscript. This research has been financed by the French National Research
592 Agency (Agence National de la Recherche), under project MODULATE, grant number ANR-18-
593 CE22-0017.

594 **References**

- 595 [1] B. Gutenberg, “Effects of Ground on Earthquake Motion,” *Bull. Seismol. Soc. Am.*, vol.
596 47, no. 3, pp. 221–250, 1957.
- 597 [2] K. Aki and K. L. Larner, “Surface Motion of a Layered Medium Having an Irregular
598 Interface Due to Incident Plane SH Waves,” *J. Geophys. Res.*, vol. 75, no. 5, pp. 933–954,
599 1970.
- 600 [3] P.-Y. Bard and M. Bouchon, “The Seismic Response of Sediment-Filled Valleys. Part 1.
601 The Case of Incident SH Waves,” *Bull. Seismol. Soc. Am.*, vol. 70, no. 4, pp. 1263–1286,
602 1980.

- 603 [4] P.-Y. Bard and M. Bouchon, "The Seismic Response of Sediment-Filled Valleys. Part 2.
604 The Case of Incident P and SV Waves," *Bull. Seismol. Soc. Am.*, vol. 70, no. 5, pp. 1921–
605 1941, 1980.
- 606 [5] J. L. King and B. E. Tucker, "Observed Variations of Earthquake Motion across a
607 Sediment-Filled Valley," *Bull. Seismol. Soc. Am.*, vol. 74, no. 1, pp. 137–151, 1984.
- 608 [6] A. S. Papageorgiou and J. Kim, "Study of the propagation and amplification of seismic
609 waves in Caracas Valley with reference to the 29 July 1967 earthquake: SH waves," *Bull.*
610 *Seismol. Soc. Am.*, vol. 81, no. 6, pp. 2214–2233, 1991.
- 611 [7] J. F. Hall and J. L. Beck, "Structural Damage in Mexico City," *Geophys. J. Int.*, vol. 13,
612 no. 6, pp. 589–592, 1986.
- 613 [8] R. W. Graves, "Modeling Three-Dimensional Site Response Effects in the Marina District
614 Basin, San Francisco, California," *Bull. Seismol. Soc. Am.*, vol. 83, no. 4, pp. 1042–1063,
615 1993.
- 616 [9] H. Kawase, "The cause of the damage belt in Kobe: 'The basin-edge effect,' constructive
617 interference of the direct S-wave with the basin-induced diffracted/Rayleigh waves,"
618 *Seismol. Res. Lett.*, vol. 67, no. 5, pp. 25–34, 1996.
- 619 [10] A. Frankel, W. Stephenson, and D. Carver, "Sedimentary basin effects in Seattle,
620 Washington: Ground-motion observations and 3D simulations," *Bull. Seismol. Soc. Am.*,
621 vol. 99, no. 3, pp. 1579–1611, 2009.
- 622 [11] K. Koketsu, K. Hatayama, T. Furumura, Y. Ikegami, and S. Akiyama, "Damaging Long-
623 period Ground Motions from the 2003 Mw 8.3 Tokachi-oki, Japan Earthquake," *Seismol.*
624 *Res. Lett.*, vol. 76, no. 1, pp. 67–73, 2005.

- 625 [12] K. Hatayama, T. Kanno, and K. Kudo, "Control factors of spatial variation of long-period
626 strong ground motions in the Yufutsu sedimentary basin, Hokkaido, during the Mw 8.0
627 2003 Tokachi-oki, Japan, earthquake," *Bull. Seismol. Soc. Am.*, vol. 97, no. 4, pp. 1308–
628 1323, 2007.
- 629 [13] M. Çelebi, I. Okawa, T. Kashima, S. Koyama, and M. Iiba, "Response of a tall building far
630 from the epicenter of the 11 March 2011 M9.0 Great East Japan earthquake and
631 aftershocks," *Struct. Des. Tall Spec. Build.*, vol. 24, no. July 2014, pp. 421–439, 2014.
- 632 [14] T. Furumura and T. Hayakawa, "Anomalous propagation of long-period ground motions
633 recorded in Tokyo during the 23 October 2004 Mw 6.6 Niigata-ken Chuetsu, Japan,
634 earthquake," *Bull. Seismol. Soc. Am.*, vol. 97, no. 3, pp. 863–880, 2007.
- 635 [15] S. Kinoshita, H. Fujiwara, T. Mikoshiba, and T. Hoshino, "Secondary Love waves
636 observed by a strong-motion array in the Tokyo lowlands, Japan," *J. Phys. Earth*, vol. 40,
637 no. 1, pp. 99–116, 1992.
- 638 [16] K. Kato, K. Aki, and T. L. Teng, "3-D simulations of surface wave propagation in the
639 Kanto sedimentary basin, Japan - part 1: application of the surface wave Gaussian beam
640 method," *Bull. - Seismol. Soc. Am.*, vol. 83, no. 6, pp. 1676–1699, 1993.
- 641 [17] K. Hatayama, K. Matsunami, T. Iwata, and K. Irikura, "Basin-Induced Love Waves of the
642 Osaka in the Eastern Basin," *J. Phys. Earth*, vol. 43, pp. 131–155, 1995.
- 643 [18] K. Miyakoshi, M. Horike, and R. Nakamiya, "Long predominant period map and detection
644 of resonant high-rise buildings in the Osaka Basin, western Japan," *Bull. Seismol. Soc.*
645 *Am.*, vol. 103, no. 1, pp. 247–257, 2013.
- 646 [19] K. Sato, K. Asano, and T. Iwata, "Long-period Ground Motion Characteristics of the

- 647 Osaka Sedimentary Basin during the 2011 Great Tohoku Earthquake,” in *15 WCEE*, 2012,
648 pp. 0–6.
- 649 [20] K. Asano *et al.*, “Modelling of wave propagation and attenuation in the Osaka sedimentary
650 basin, western Japan, during the 2013 Awaji Island earthquake,” *Geophys. J. Int.*, vol. 204,
651 no. 3, pp. 1678–1694, 2016.
- 652 [21] K. B. Olsen, “Site Amplification in the Los Angeles Basin from Three-Dimensional
653 Modeling of Ground Motion,” *Bull. Seismol. Soc. Am.*, vol. 90, no. 6B, pp. S77–S94,
654 2000.
- 655 [22] M. A. Denolle, H. Miyake, S. Nakagawa, N. Hirata, and G. C. Beroza, “Long-period
656 seismic amplification in the Kanto Basin from the ambient seismic field,” *Geophys. Res.*
657 *Lett.*, vol. 41, pp. 2319–2325, 2014.
- 658 [23] M. Horike, H. Uebayashi, and Y. Takeuchi, “Seismic Response in Three-Dimensional
659 Sedimentary Basin due to Plane S Wave Incidence,” *J. Phys. Earth*, vol. 38, no. 4, pp.
660 261–284, 1990.
- 661 [24] S. Takemura, M. Akatsu, K. Masuda, K. Kajikawa, and K. Yoshimoto, “Long-period
662 ground motions in a laterally inhomogeneous large sedimentary basin : observations and
663 model simulations of long-period surface waves in the northern Kanto Basin , Japan,”
664 *Earth, Planets Sp.*, vol. 67, no. 33, pp. 1–17, 2015.
- 665 [25] L. Viens, H. Miyake, and K. Koketsu, “Simulations of long-period ground motions from a
666 large earthquake using finite rupture modeling and the ambient seismic field,” *J. Geophys.*
667 *Res. Solid Earth*, vol. 121, no. 12, pp. 8774–8791, 2016.
- 668 [26] L. Seydoux, N. M. Shapiro, J. De Rosny, and M. Landès, “Spatial coherence of the seismic

- 669 wavefield continuously recorded by the USArray,” *Geophys. Res. Lett.*, vol. 43, pp. 9644–
670 9652, 2016.
- 671 [27] M. Wathelet, B. Guillier, P. Roux, C. Cornou, and M. Ohrnberger, “Rayleigh wave three-
672 component beamforming: signed ellipticity assessment from high-resolution frequency-
673 wavenumber processing of ambient vibration arrays,” *Geophys. J. Int.*, vol. 215, no. 1, pp.
674 507–523, 2018.
- 675 [28] B. E. Tucker and J. L. King, “Dependence of sediment - filled valley response on input
676 amplitude and valley properties,” *Bull. - Seismol. Soc. Am.*, vol. 74, no. 1, pp. 153–165,
677 1984.
- 678 [29] H.-L. Liu and T. Heaton, “Array analysis of the ground velocities and accelerations from
679 the 1971 San Fernando, California, earthquake,” *Bull. Seismol. Soc. Am.*, vol. 74, no. 5, pp.
680 1951–1968, 1984.
- 681 [30] T. C. Hanks, “Strong Ground Motion of the San Fernando, California, Earthquake: Ground
682 Displacements,” *Bull. Seismol. Soc. Am.*, vol. 65, no. 1, pp. 193–225, 1975.
- 683 [31] J. S. Barker, M. Campillo, F. J. Sánchez-Sesma, D. Jongmans, and S. K. Singh, “Analysis
684 of wave propagation in the Valley of Mexico from a dense array of seismometers,” *Bull.*
685 *Seismol. Soc. Am.*, vol. 86, no. 6, pp. 1667–1680, 1996.
- 686 [32] E. Fukuyama and T. Mikumo, “Dynamic rupture propagation during the 1891 Nobi,
687 Central Japan, earthquake: A possible extension to the branched faults,” *Bull. Seismol. Soc.*
688 *Am.*, vol. 96, no. 4 A, pp. 1257–1266, 2006.
- 689 [33] H. Sekiguchi and M. Yoshimi, “Broadband Ground Motion Reconstruction for the Kanto
690 Basin during the 1923 Kanto Earthquake,” *Pure Appl. Geophys.*, vol. 168, no. 3–4, pp.

- 691 609–630, 2011.
- 692 [34] K. C. Meza-Fajardo, A. S. Papageorgiou, and J. F. Semblat, “Identification and extraction
693 of surface waves from three-component seismograms based on the normalized inner
694 product,” *Bull. Seismol. Soc. Am.*, vol. 105, no. 1, pp. 210–229, 2015.
- 695 [35] K. Ueshita and T. Sato, “Study on Subsidence of the Nōbi Plain,” in *10th International
696 Conference on Soil Mechanics and Foundation Engineering (Stockholm). Environmental
697 Control (incl Waste Materials).*, 1981.
- 698 [36] K. X.-S. Hao and H. Fujiwara, “Sedimentary Thickness In The Eastern Kanto Basin
699 Estimated By All-Pass Receiver Function Using Dense Earthquake,” *14th World Conf.
700 Earthq. Eng.*, pp. 10–15, 2008.
- 701 [37] NIED, “National Research Institute for Earth Science and Disaster Resilience, K-net, Kik-
702 net,” 2019. .
- 703 [38] K. Yoshimoto and S. Takemura, “A study on the predominant period of long-period
704 ground motions in the Kanto Basin , Japan,” *Earth, Planets Sp.*, vol. 66, no. 100, pp. 1–7,
705 2014.
- 706 [39] S. Kinoshita, “Kyoshin Net (K-NET),” *Seismol. Res. Lett.*, vol. 69, no. 4, pp. 309–332,
707 1998.
- 708 [40] R. G. Stockwell, L. Mansinha, and R. P. Lowe, “Localization of the Complex Spectrum:
709 The S Transform,” *IEEE Trans. Signal Process.*, vol. 44, no. 4, pp. 998–1001, 1996.
- 710 [41] R. N. Bracewell, “The Fourier Transform and applications,” *McGraw Hill*, pp. 1–10, 2000.
- 711 [42] T. Furumura *et al.*, “Strong ground motions from the 2011 earthquake obtained from a
712 dense nationwide seismic network,” *Recent Landslides*, vol. 8, pp. 333–338, 2011.

- 713 [43] A. Frankel, “Rupture History of the 2011 M 9 Tohoku Japan Earthquake Determined from
714 Strong-Motion and High-Rate GPS Recordings : Subevents Radiating Energy in Different
715 Frequency Bands,” *Bull. Seismol. Soc. Americ*, vol. 103, no. 2, pp. 1290–1306, 2013.
- 716 [44] H. Kubo and Y. Kakehi, “Source process of the 2011 Tohoku earthquake estimated from
717 the joint inversion of teleseismic body waves and geodetic data including seafloor
718 observation data: Source model with enhanced reliability by using objectively determined
719 inversion settings,” *Bull. Seismol. Soc. Am.*, vol. 103, no. 2B, pp. 1195–1220, 2013.
- 720 [45] K. C. Meza-Fajardo and A. S. Papageorgiou, “Estimation of rocking and torsion associated
721 with surface waves extracted from recorded motions,” *Soil Dyn. Earthq. Eng.*, vol. 80,
722 2016.
- 723 [46] H. Miyake and K. Koketsu, “Long-period ground motions from a large offshore
724 earthquake: The case of the 2004 off the Kii peninsula earthquake, Japan,” *Earth, Planets
725 Sp.*, vol. 57, pp. 203–207, 2005.
- 726 [47] K. B. Olsen *et al.*, “TeraShake2: Spontaneous rupture simulations of Mw 7.7 earthquakes
727 on the Southern San Andreas fault,” *Bull. Seismol. Soc. Am.*, vol. 98, no. 3, pp. 1162–1185,
728 2008.
- 729 [48] K. C. Meza-Fajardo and A. S. Papageorgiou, “Response of tall buildings to base rocking
730 induced by Rayleigh waves,” no. January, pp. 1–19, 2018.
- 731 [49] P. Boué, M. Denolle, N. Hirata, S. Nakagawa, and G. C. Beroza, “Beyond basin
732 resonance : Characterizing wave propagation using a dense array and the ambient seismic
733 field,” *Geophys. J. Int.*, vol. 206, no. 2, pp. 1261–1272, 2016.
- 734 [50] T. Tanimoto and L. Rivera, “Prograde Rayleigh wave particle motion,” vol. 1, pp. 399–

- 735 405, 2005.
- 736 [51] K. Koketsu and M. Kikuchi, "Propagation of Seismic Ground Motion in the Kanto Basin ,
737 Japan," vol. 288, no. May, pp. 1237–1240, 2000.
- 738 [52] Y. Cao, K. C. Meza-Fajardo, G. P. Mavroeidis, and A. S. Papageorgiou, "Effects of wave
739 passage on torsional response of symmetric buildings subjected to near-fault pulse-like
740 ground motions," *Soil Dyn. Earthq. Eng.*, vol. 88, pp. 109–123, 2016.
- 741 [53] R. Gendrin *et al.*, "Wave packet propagation in an amplifying medium and its application
742 to the dispersion characteristics and to the generation mechanisms of Pc 1 events," *Planet.
743 Space Sci.*, vol. 19, no. 2, pp. 165–194, 1971.
- 744 [54] M. B. Priestley, "Some Notes on the Physical Interpretation of Spectra of Non-Stationary
745 Stochastic Processes," *J. Sound Vib.*, vol. 17, no. 1, pp. 51–54, 1971.
- 746 [55] M. B. Priestley, "Evolutionary Spectra and Non-Stationary Processes," *J. R. Stat. Soc. Ser.
747 B*, vol. 27, no. 2, pp. 204–237, 1965.
- 748 [56] W. B. Joyner, "Strong motion from surface waves in deep sedimentary basins," *Bull.
749 Seismol. Soc. Am.*, vol. 90, no. 6 SUPPL., pp. 95–112, 2000.
- 750 [57] K. Yoshimoto and S. Takemura, "Surface wave excitation at the northern edge of the
751 Kanto Basin, Japan," *Earth, Planets Sp.*, vol. 66, no. 1, pp. 1–7, 2014.
- 752 [58] Y. Mukai, T. Furumura, and T. Maeda, "Causes of Azimuthally Dependent Amplification
753 Variations of Long-period Ground Motions in the Kanto Basin, Central Japan," *Bull.
754 Earthq. Res. Inst.*, vol. 93, pp. 31–48, 2018.
- 755 [59] T. Uetake, "Effects of subsurface structures of source regions on long - period ground
756 motions observed in the Tokyo Bay area , Japan," *Earth, Planets Sp.*, 2017.

757 [60] R. Tajima and F. Tajima, “Seismic scaling relation of the 2007 Off Mid Niigata, Japan,
758 earthquake (Mw 6.6) sequence in comparison with two other earthquake (Mw 6.6)
759 sequences,” *Earth, Planets Sp.*, vol. 60, pp. 1137–1141, 2008.

760

761 **Authors Affiliations**

762 Kristel C. Meza-Fajardo

763 Risk and Prevention Division, BRGM.

764 3, avenue Claude-Guillemin, BP 36009 - 45060 Orléans cedex 2 – FRANCE

765 Tel: +33 (0) 2 38 64 36 91

766 E-mail: k.meza@brgm.fr

767

768 Hideo Aochi

769 Risk and Prevention Division, BRGM.

770 3, avenue Claude-Guillemin, BP 36009 - 45060 Orléans cedex 2 – FRANCE

771 E-mails: h.aochi@brgm.fr

772

773 Apostolos S. Papageorgiou

774 Department of Civil Engineering, University of Patras

775 GR-26500 Patras, Greece.

776 E-mail: papaga@upatras.gr

777 **List of Figure Captions**

778 Figure 1. The Nobi and Kanto basins. (a) Location of the basins (indicated by the squares), and
779 locations of the epicenters of the events (indicated by stars), considered in this study. (b) Spatial
780 distribution of K-NET stations in the Nobi basin. (c) Spatial distribution of K-NET stations in the
781 Kanto basin. The contour plots indicate the depth corresponding to $V_s=2700$ m/s, with a level
782 step of 500 m. For clarity, stations at Tokyo bay are not shown in (c). The stations codes at the
783 Chiba sub-basin start with the letters CHB, at the Gunma-Saitama area with the letters GNM or
784 SIT, and at the Tokyo bay area with letter TKY.

785 Figure 2. 3D deep structure model for a $V_s=2700$ m/s provided by NIED for (a) Kanto basin, and
786 (b) Nobi basin. Whereas the Nobi basin apparently can be characterized as consisting of a single
787 sub-basin, we can observe that the Kanto basin is composed of several sub-basins.

788 Figure 3. Displacement waveforms at rock stations during three different events. (a) Station
789 SIT006 at Kanto basin, and (b) station GIF024 at Nobi basin. Zero pads have been added at the
790 end of the recordings so that all time-histories have the same time length.

791 Figure 4. Amplitudes of the S-transform of vertical components recorded during three different
792 events. (a) Station SIT006 at Kanto basin, and (b) station GIF024 at Nobi basin. We can observe
793 the similarities in frequency content of the two Chuetsu events, with dominant frequencies
794 between 0.1 and 0.2 Hz, at the two stations. For the Tohoku earthquake the dominant frequency
795 at both stations evidently is below 0.1 Hz.

796 Figure 5. Extracted Rayleigh waves in the frequency range 0.05-0.1 Hz during the 2011 Tohoku
797 earthquake propagating to the west in the Nobi basin. (a) Retrograde waves propagating to the
798 West, (b) Retrograde waves propagating to the East. The direction of polarization in the
799 horizontal component at each station is indicated on the top panels by the arrows. On the bottom

800 we display the time-histories of the horizontal and vertical components of extracted wave trains.
801 The time-history of the vertical component has been shifted 90 degrees with respect to the
802 horizontal component.

803 Figure 6. Extracted retrograde Rayleigh waves in the frequency range 0.05-0.1 Hz during the
804 2011 Tohoku earthquake propagating to the west in the Nobi basin. The direction of polarization
805 in the horizontal component at each station is indicated on the top panels by the arrows. On the
806 bottom we display the time-histories of the horizontal and vertical components of extracted wave
807 trains. The time-history of the vertical component has been shifted 90 degrees with respect to the
808 horizontal component.

809 Figure 7. Extracted Love waves in the range 0.05-0.1 Hz in Kanto basin during the 2011 Tohoku
810 earthquake in the Chiba area. The direction of polarization in the horizontal component at each
811 station is shown on the left panel. The right panel shows the time histories of the horizontal
812 component. In the case of Love waves, the direction of propagation is expected to be normal to
813 the direction of polarization.

814 Figure 8. Extracted Rayleigh waves in the frequency range 0.1-0.5 Hz during the 2011 Tohoku
815 earthquake. (a) Retrograde waves in the Kanto basin, (b) Prograde waves in the Kanto basin.

816 Figure 9. Extracted Retrograde Rayleigh waves in the frequency range 0.1-0.5 Hz during the
817 2011 Tohoku earthquake.

818 Figure 10. Particle motion of extracted Rayleigh waves in the R-Z plane during Tohoku
819 earthquake for 0.1-0.5 Hz. (a) Ellipse of retrograde Rayleigh wave at station SIT001 during 120-
820 140 s, (b) Ellipse of prograde Rayleigh wave at station CHB006 during 130-150 s. R (for 'radial')
821 denotes direction of maximum energy or direction of propagation, and Z denotes the vertical
822 direction.

823 Figure 11. Extracted Love waves in the range 0.1-0.5 Hz in Kanto basin during the 2011 Tohoku
824 earthquake. The direction of polarization in the horizontal component at each station is shown on
825 the left panel. The right panel shows the time histories of the horizontal component.

826 Figure 12. Amplification and central frequency of prograde waves in the range 0.1-0.5 Hz in
827 Kanto basin during the 2011 Tohoku earthquake. (a) Central frequency of extracted waves, (b)
828 Amplification coefficient $A1$.

829 Figure 13. Amplification and central frequency of Love waves in the range 0.1-0.5 Hz in Kanto
830 basin during the 2011 Tohoku earthquake. (a) Central frequency (Hz), (b) Amplification
831 coefficient $A1$.

832 Figure 14. Amplification of surface waves in the range 0.1-0.5 Hz in Kanto basin during the 2011
833 Tohoku earthquake. (a) Time delay for prograde Rayleigh waves (s), (b) Amplification
834 coefficient $A2$ for prograde Rayleigh waves, (c) Time delay for Love waves (s), (d)
835 Amplification coefficient $A2$ for Love waves.

836 Figure 15. Retrograde Rayleigh waves in the Nobi basin extracted in the frequency range 0.1-0.5
837 Hz. (a) During the Chuetsu earthquake, (b) during the Chuetsu-oki earthquake.

838 Figure 16. Retrograde Rayleigh waves in the Kanto basin extracted in the frequency range 0.1-0.5
839 Hz. (a) During the Chuetsu earthquake, (b) during the Chuetsu-oki earthquake.

840 Figure 17. Prograde Rayleigh waves in the Kanto basin extracted in the frequency range 0.1-0.5
841 Hz. (a) During the Chuetsu earthquake, (b) during the Chuetsu-oki earthquake.

842 Figure 18. Love waves in the Kanto basin extracted in the frequency range 0.1-0.5 Hz. (a) During
843 the Chuetsu earthquake, (b) during the Chuetsu-oki earthquake.

844 Figure 19. Amplification of prograde Rayleigh waves in the Kanto basin extracted in the
845 frequency range 0.1-0.5 Hz. (a) Central frequency (Hz) during the Chuetsu earthquake, (b)

846 Central frequency (Hz) during the Chuetsu-oki earthquake, (c) Amplification coefficient A_1
847 during the Chuetsu earthquake, (d) Amplification coefficient A_1 during the Chuetsu-oki
848 earthquake.

849 Figure 20. Amplification of Love waves in the Kanto basin extracted in the frequency range 0.1-
850 0.5 Hz. (a) Central frequency (Hz) during the Chuetsu earthquake, (b) Central frequency (Hz)
851 during the Chuetsu-oki earthquake, (c) Amplification coefficient A_1 during the Chuetsu
852 earthquake, (d) Amplification coefficient A_1 during the Chuetsu-oki earthquake.
853

Table 1. Earthquake events considered for surface wave analysis in Nobi and Kanto basins. Earthquake information is based on the catalogue of the Japan Meteorological Agency. Time is local time (JST).

Name	Event time	Magnitude M _{JMA}	Latitude	Longitude	Depth (Km)	Note
Niigata-Chuetsu ⁽¹⁾	2004/10/23 17:56:00	6.8	37.291	138.867	13	Crustal reverse faulting
Chuetsu-oki ⁽²⁾	2007/07/16 10:13:22	6.8	31.557	136.608	17	Crustal reverse faulting
Tohoku ⁽³⁾	2011/03/11 14:46:18	9.0	38.103	142.86	24	subduction

⁽¹⁾ [14]

⁽²⁾ [60]

⁽³⁾ [44]

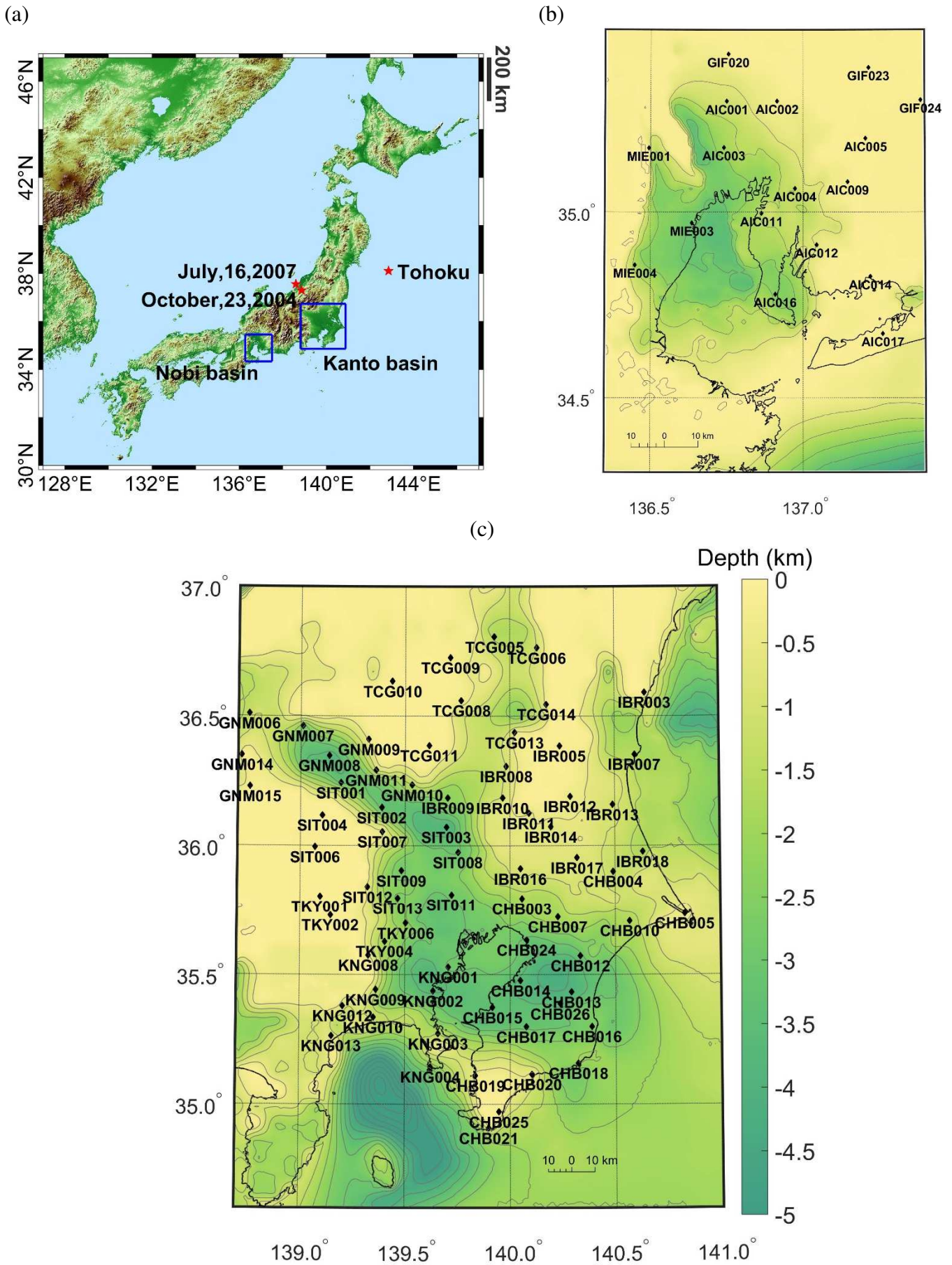


Figure 1. The Nobi and Kanto basins. (a) Location of the basins (indicated by the squares), and locations of the epicenters of the events (indicated by the stars), considered in this study. (b) Spatial distribution of K-NET stations in the Nobi basin. (c) Spatial distribution of K-NET stations in the Kanto basin. The contour plots indicate the depth corresponding to $V_s=2700$ m/s, with a level step of 500 m. For clarity, stations at Tokyo bay are not shown in (c). The stations codes at the Chiba sub-basin start with the letters CHB, at the Gunma-Saitama area with the letters GNM or SIT, and at the Tokyo bay area with letter TKY.

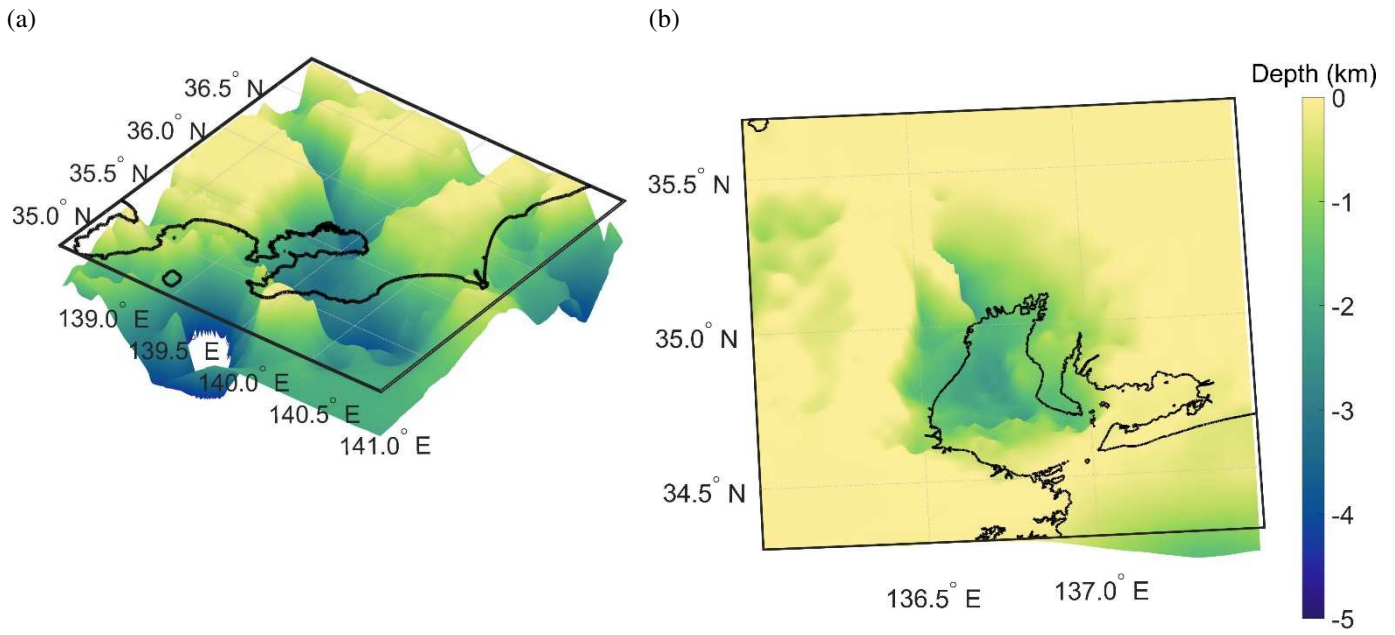


Figure 2. 3D deep structure model for a $V_s=2700$ m/s provided by NIED for (a) Kanto basin, and (b) Nobi basin. Whereas the Nobi basin apparently can be characterized as consisting of a single sub-basin, we can observe that the Kanto basin is composed of several sub-basins.

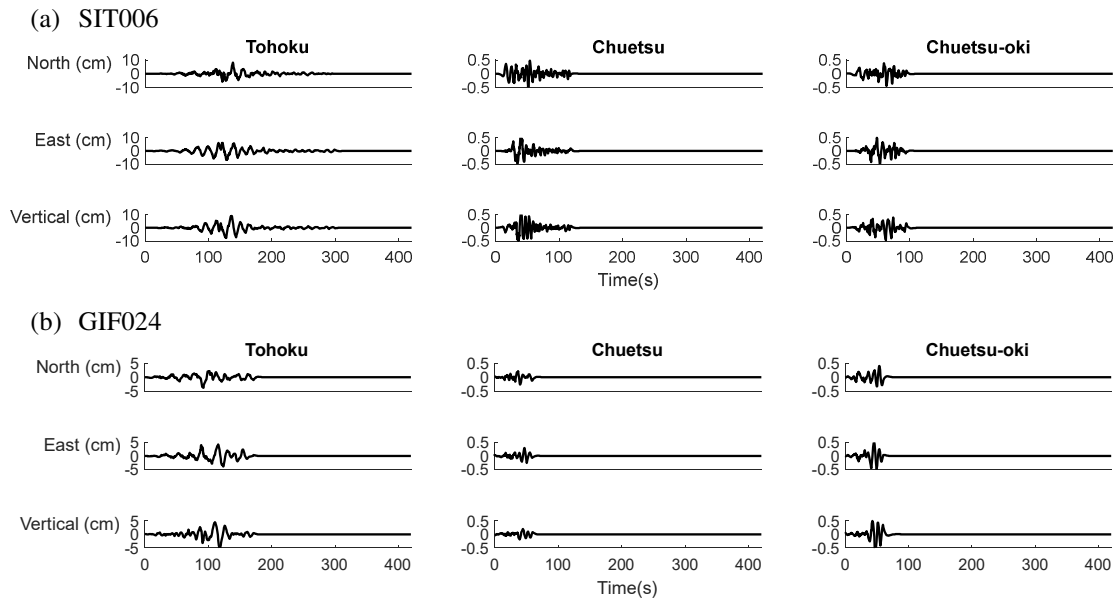


Figure 3. Displacement waveforms at rock stations during three different events. (a) Station SIT006 at Kanto basin, and (b) station GIF024 at Nobi basin. Zero pads have been added at the end of the recordings so that all time-histories have the same time length.

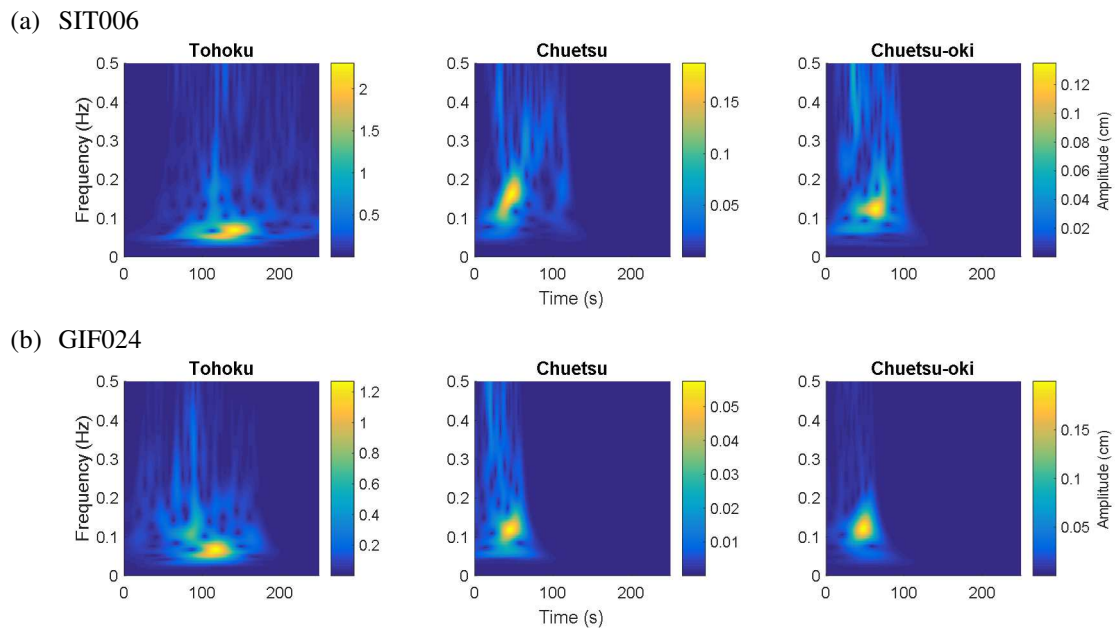


Figure 4. Amplitudes of the S-transform of vertical components recorded during three different events. (a) Station SIT006 at Kanto basin, and (b) station GIF024 at Nobi basin. We can observe the similarities in frequency content of the two Chuetsu events, with dominant frequencies between 0.1 and 0.2 Hz, at the two stations. For the Tohoku earthquake the dominant frequency at both stations evidently is below 0.1 Hz.

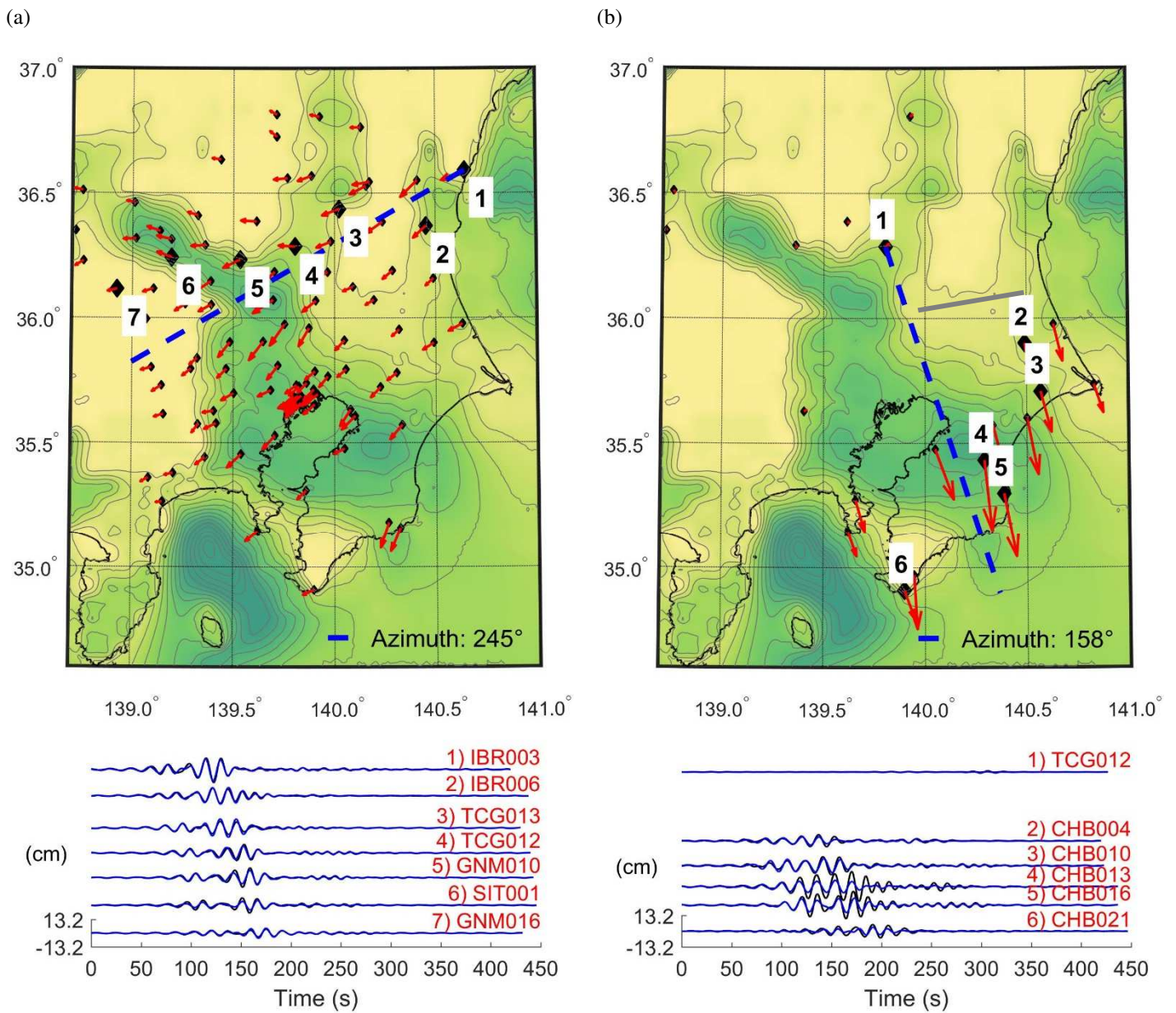


Figure 5. Extracted Rayleigh waves in the frequency range 0.05-0.1 Hz during the 2011 Tohoku earthquake propagating to the west in the Nobi basin. (a) Retrograde waves propagating to the West, (b) Retrograde waves propagating to the East. The direction of polarization in the horizontal component at each station is indicated on the top panels by the arrows. On the bottom we display the time-histories of the horizontal and vertical components of extracted wave trains. The time-history of the vertical component has been shifted 90 degrees with respect to the horizontal component.

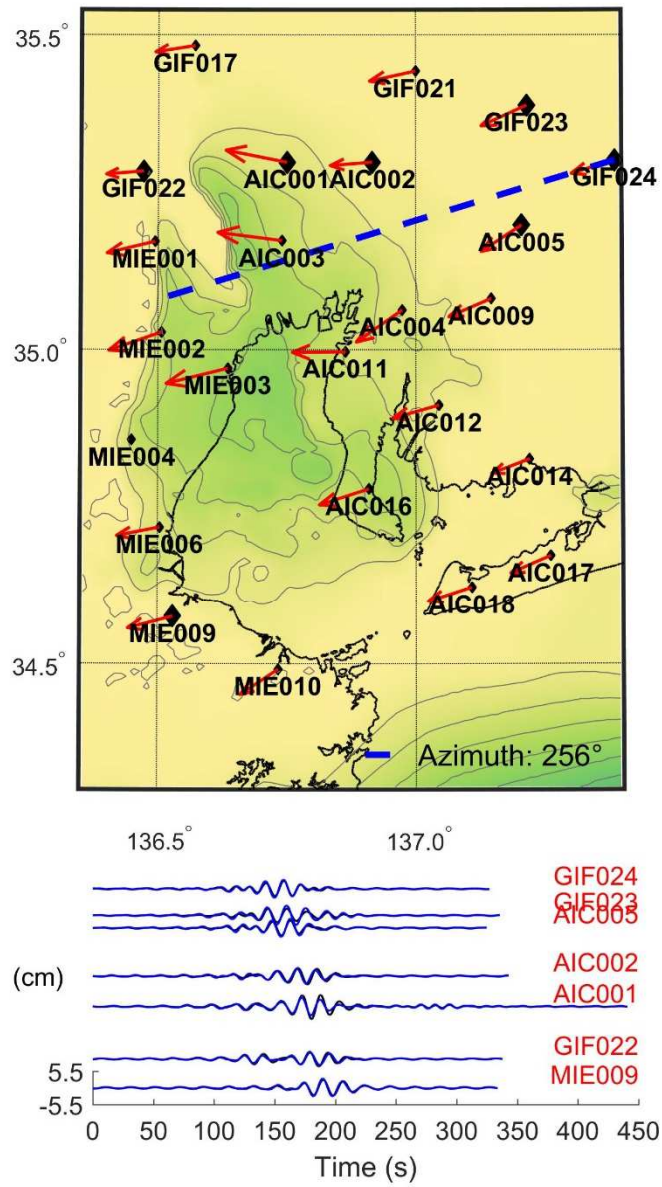


Figure 6. Extracted retrograde Rayleigh waves in the frequency range 0.05-0.1 Hz during the 2011 Tohoku earthquake propagating to the west in the Nobi basin. The direction of polarization in the horizontal component at each station is indicated on the top panels by the arrows. On the bottom we display the time-histories of the horizontal and vertical components of extracted wave trains. The time-history of the vertical component has been shifted 90 degrees with respect to the horizontal component.

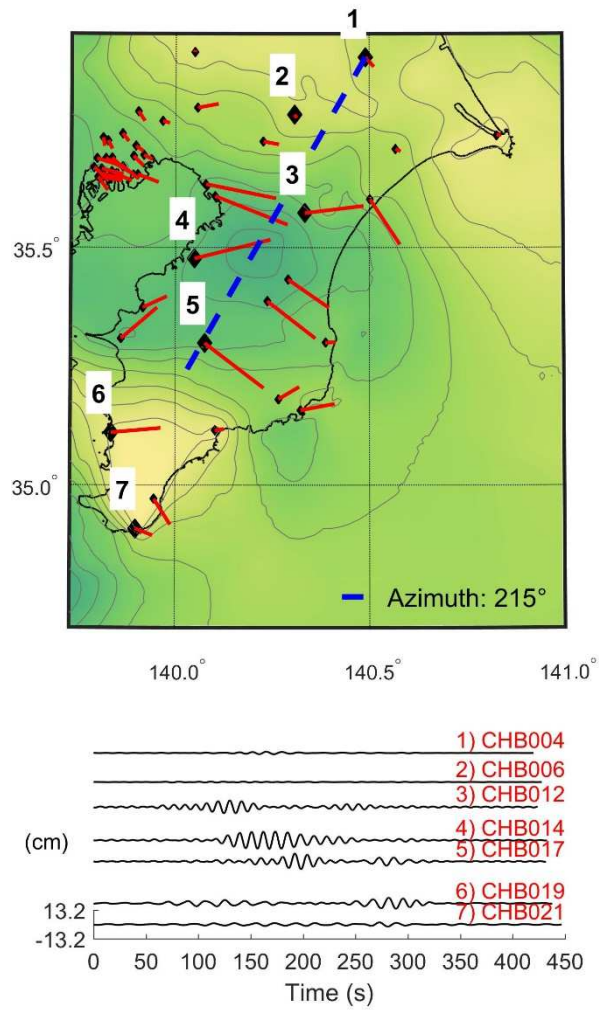


Figure 7. Extracted Love waves in the range 0.05-0.1 Hz in Kanto basin during the 2011 Tohoku earthquake in the Chiba area. The direction of polarization in the horizontal component at each station is shown on the left panel. The right panel shows the time histories of the horizontal component. In the case of Love waves, the direction of propagation is expected to be normal to the direction of polarization.

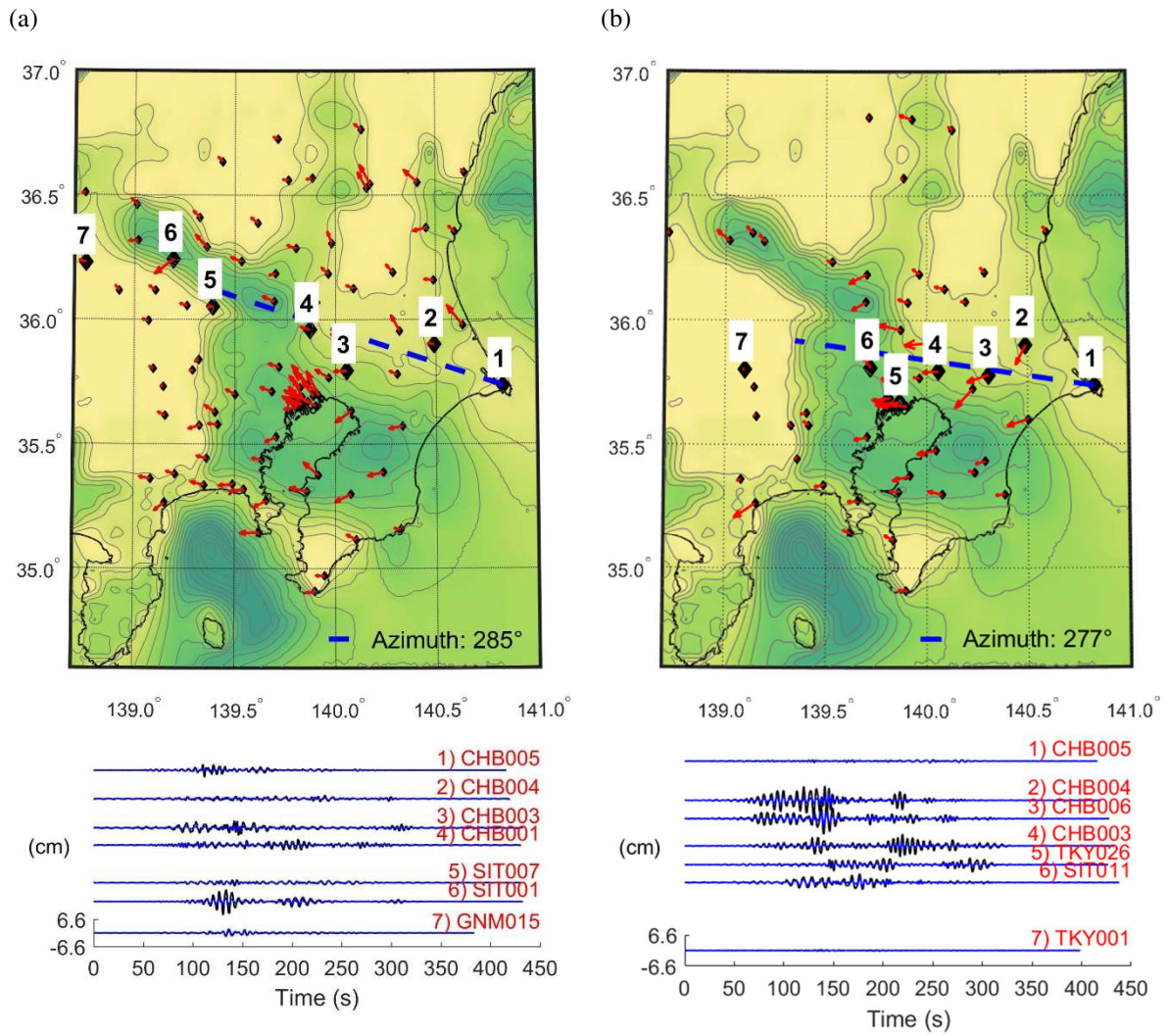


Figure 8. Extracted Rayleigh waves in the frequency range 0.1-0.5 Hz during the 2011 Tohoku earthquake. (a) Retrograde waves in the Kanto basin, (b) Prograde waves in the Kanto basin.

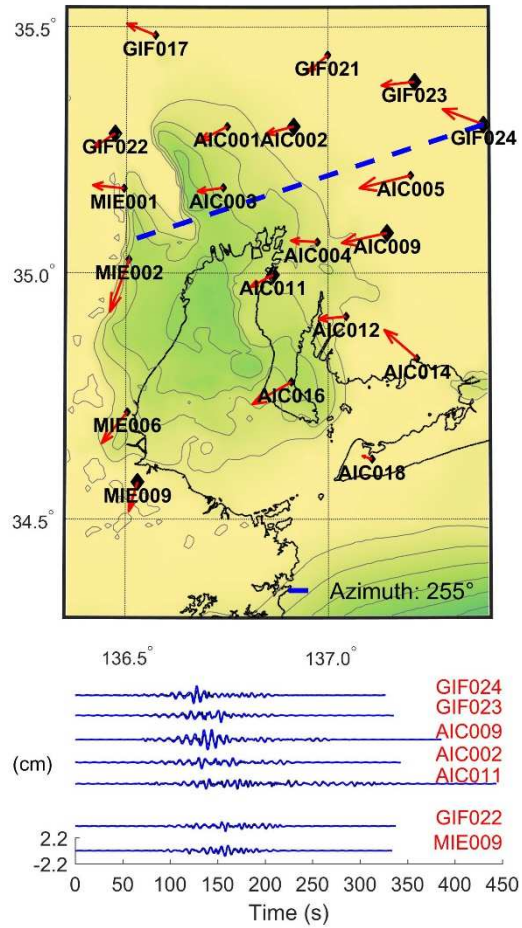


Figure 9. Extracted Retrograde Rayleigh waves in the frequency range 0.1-0.5 Hz during the 2011 Tohoku earthquake.

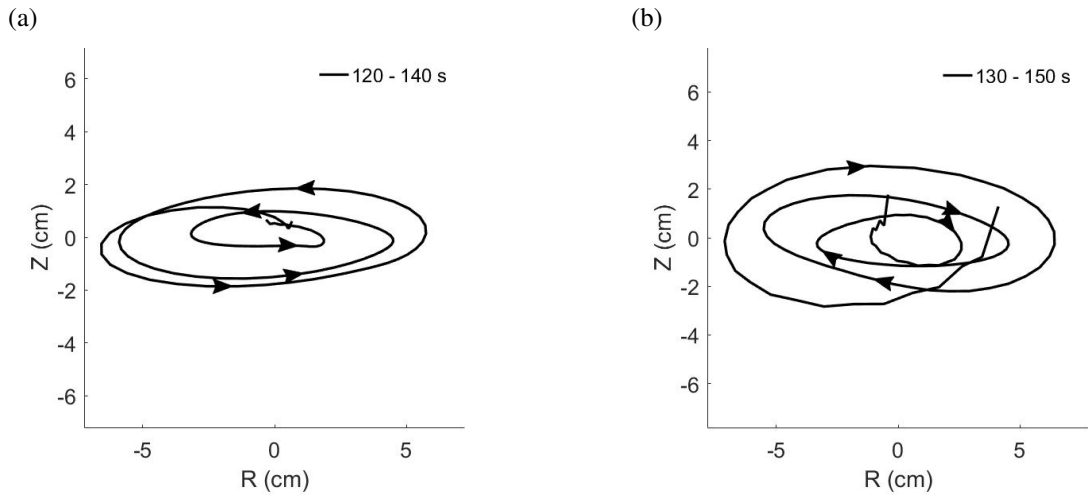


Figure 10. Particle motion of extracted Rayleigh waves in the R-Z plane during Tohoku earthquake for 0.1-0.5 Hz. (a) Ellipse of retrograde Rayleigh wave at station SIT001 during 120-140 s, (b) Ellipse of prograde Rayleigh wave at station CHB006 during 130-150 s. R (for 'radial') denotes direction of maximum energy or direction of propagation, and Z denotes the vertical direction.

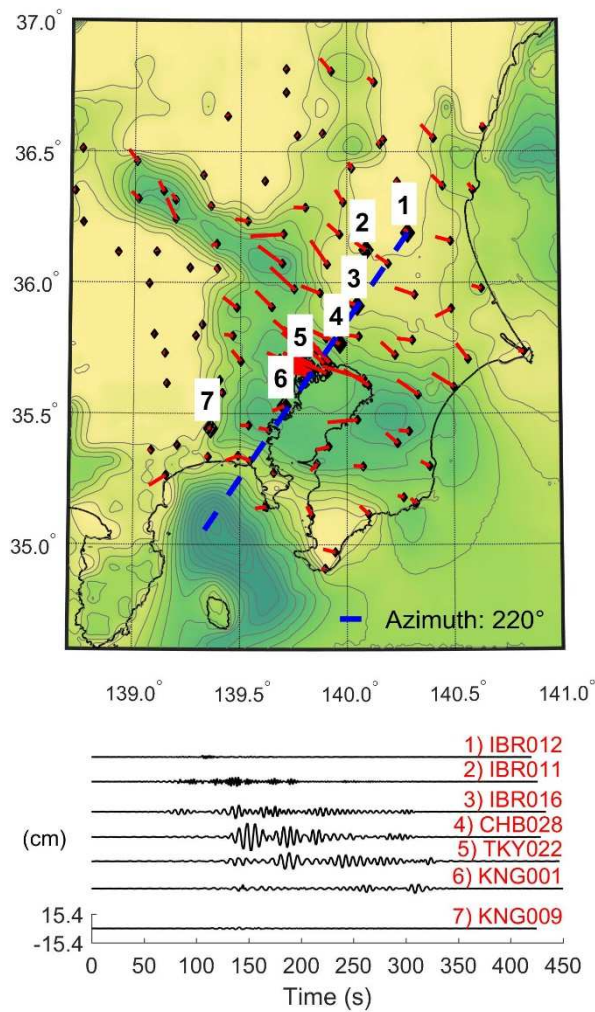


Figure 11. Extracted Love waves in the range 0.1-0.5 Hz in Kanto basin during the 2011 Tohoku earthquake. The direction of polarization in the horizontal component at each station is shown on the left panel. The right panel shows the time histories of the horizontal component.

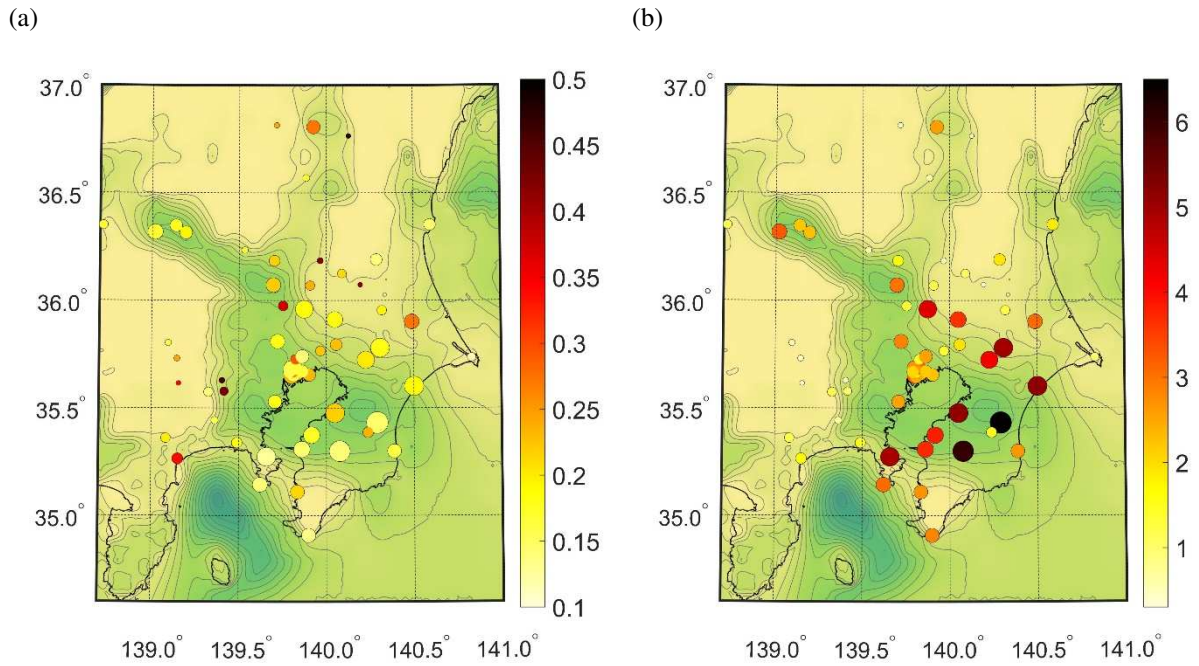


Figure 12. Amplification and central frequency of prograde waves in the range 0.1-0.5 Hz in Kanto basin during the 2011 Tohoku earthquake. (a) Central frequency of extracted waves, (b) Amplification coefficient A_1 .

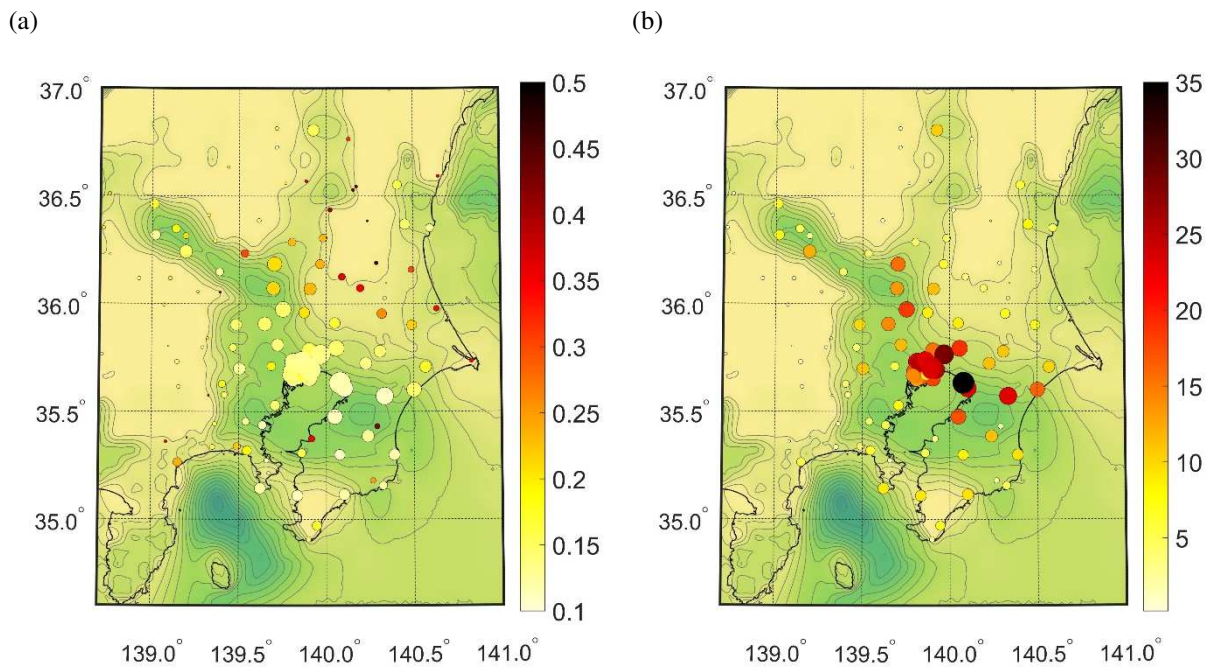


Figure 13. Amplification and central frequency of Love waves in the range 0.1-0.5 Hz in Kanto basin during the 2011 Tohoku earthquake. (a) Central frequency (Hz), (b) Amplification coefficient A_1 .

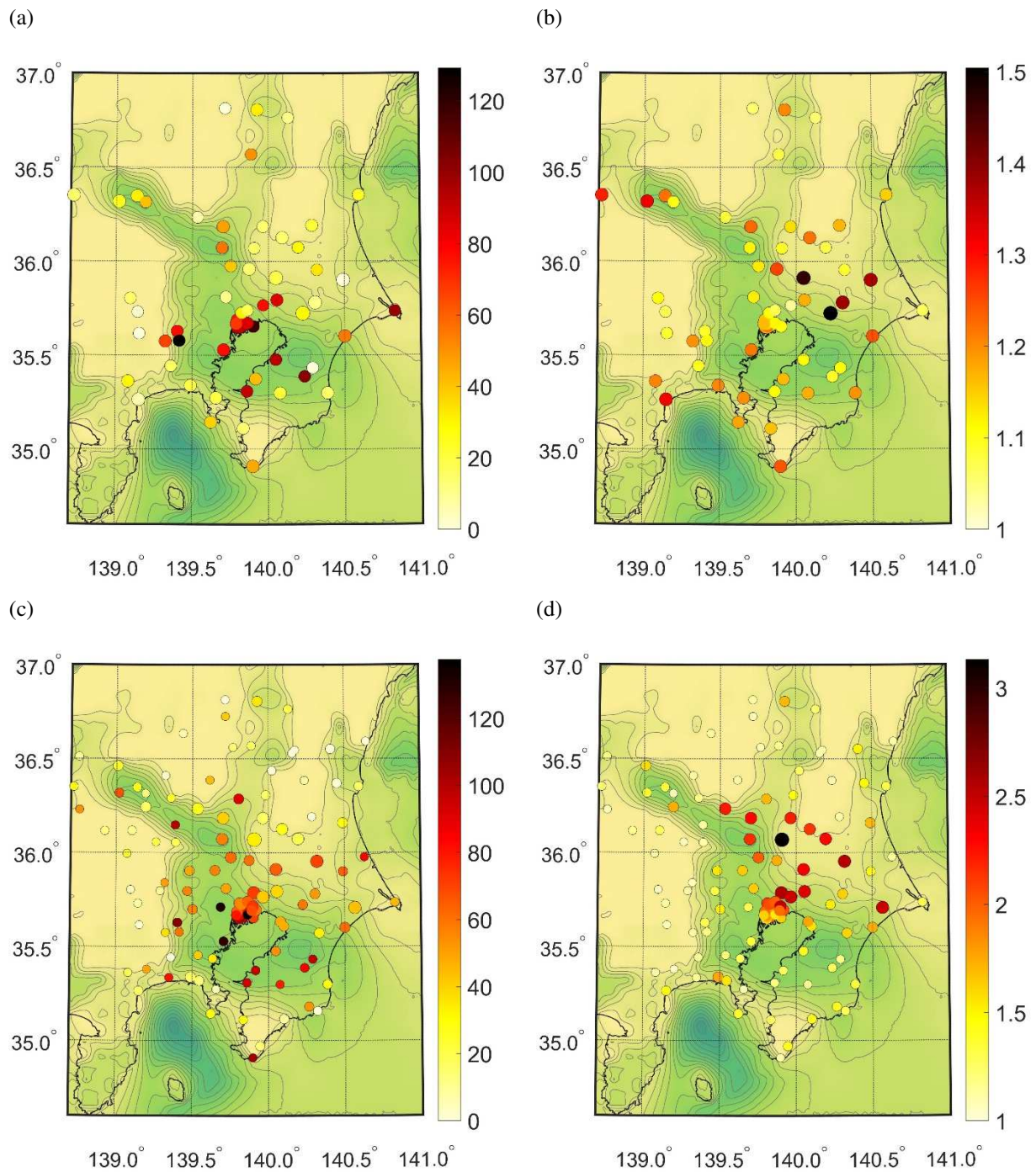
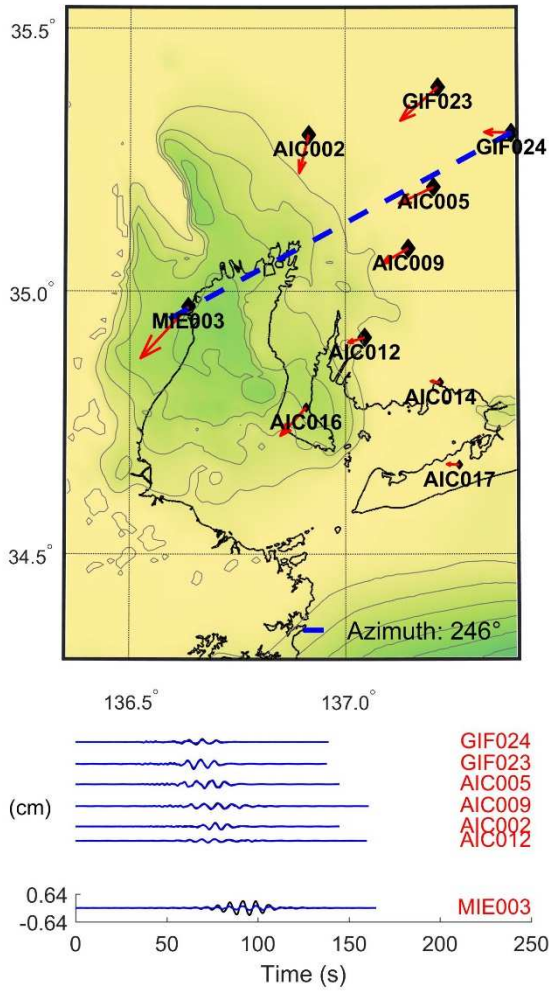


Figure 14. Amplification of surface waves in the range 0.1-0.5 Hz in Kanto basin during the 2011 Tohoku earthquake. (a) Time delay for prograde Rayleigh waves (s), (b) Amplification coefficient A_2 for prograde Rayleigh waves, (c) Time delay for Love waves (s), (d) Amplification coefficient A_2 for Love waves.

(a)



(b)

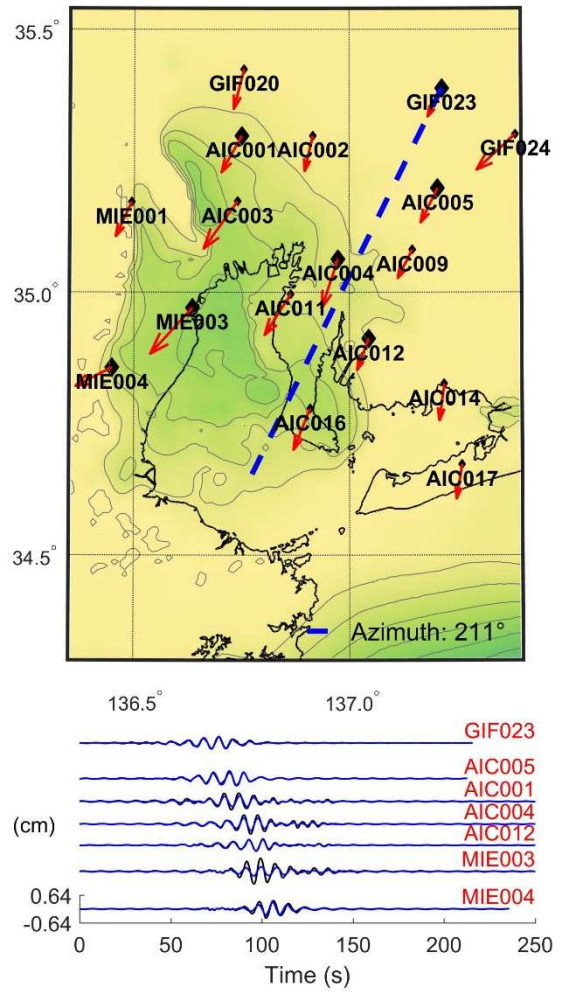
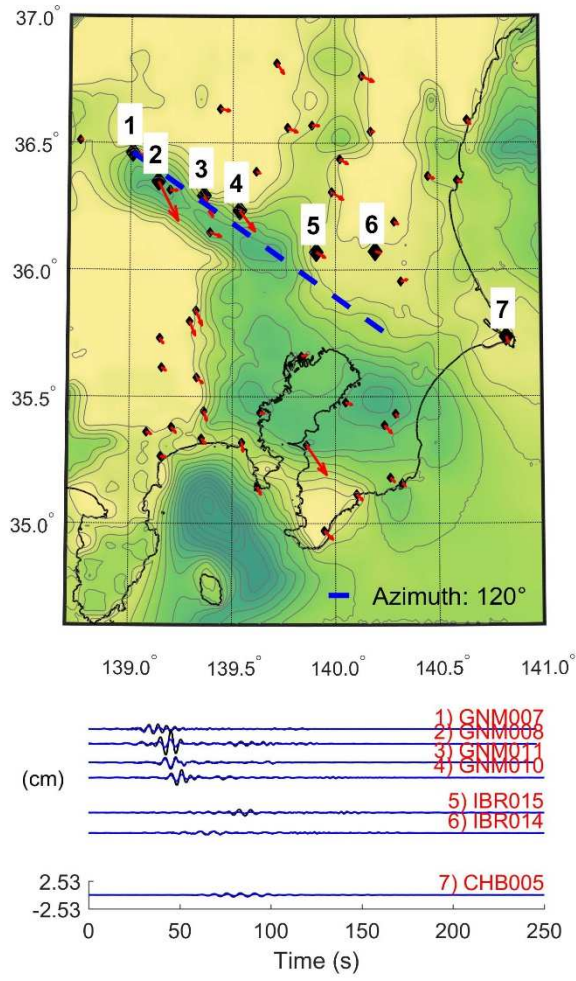


Figure 15. Retrograde Rayleigh waves in the Nobi basin extracted in the frequency range 0.1-0.5 Hz. (a) During the Chuetsu earthquake, (b) during the Chuetsu-oki earthquake.

(a)



(b)

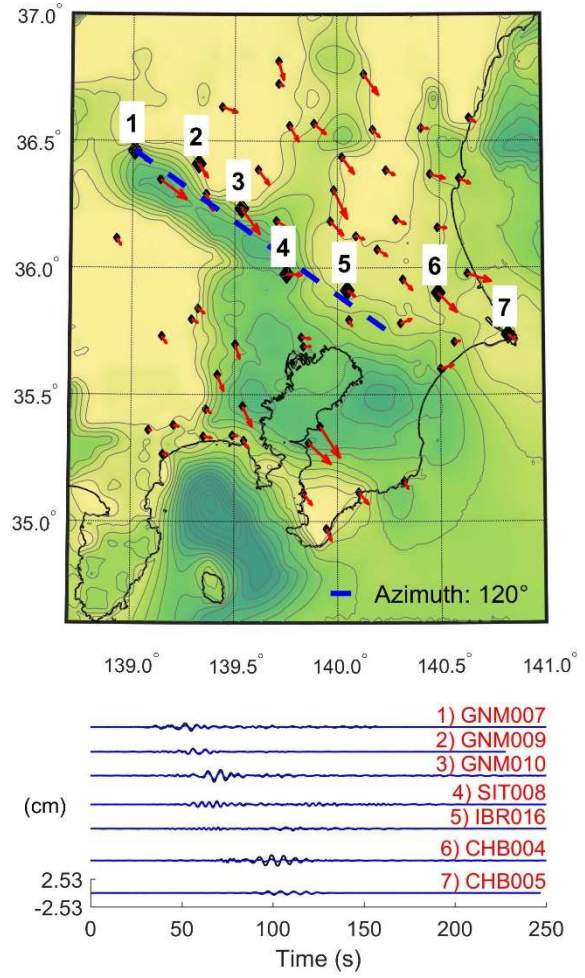
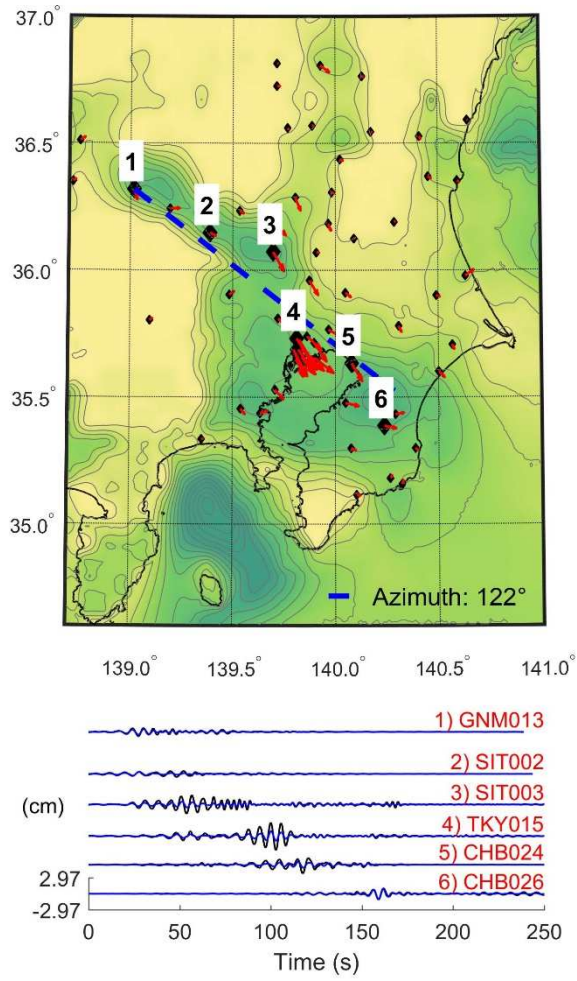


Figure 16. Retrograde Rayleigh waves in the Kanto basin extracted in the frequency range 0.1-0.5 Hz. (a) During the Chuetsu earthquake, (b) during the Chuetsu-oki earthquake.

(a)



(b)

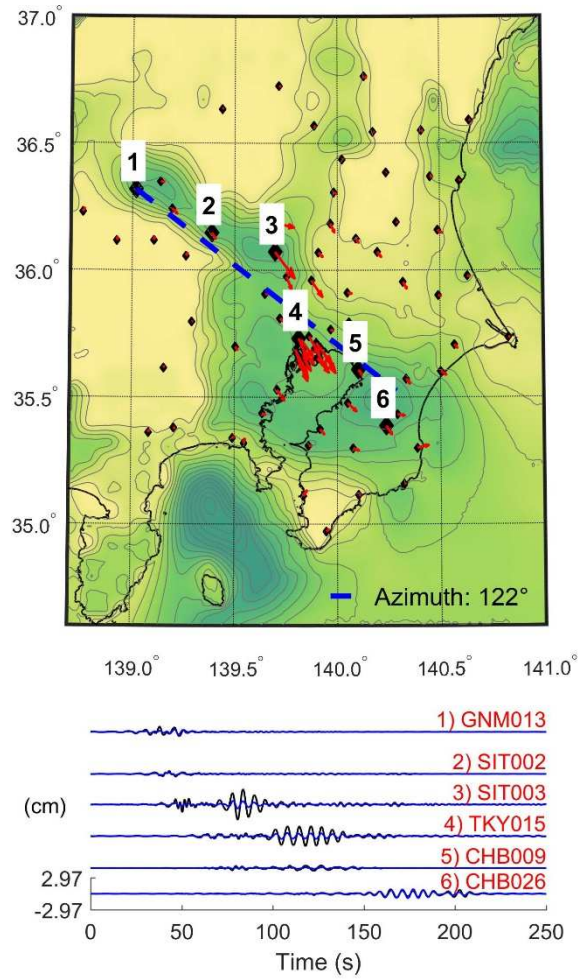
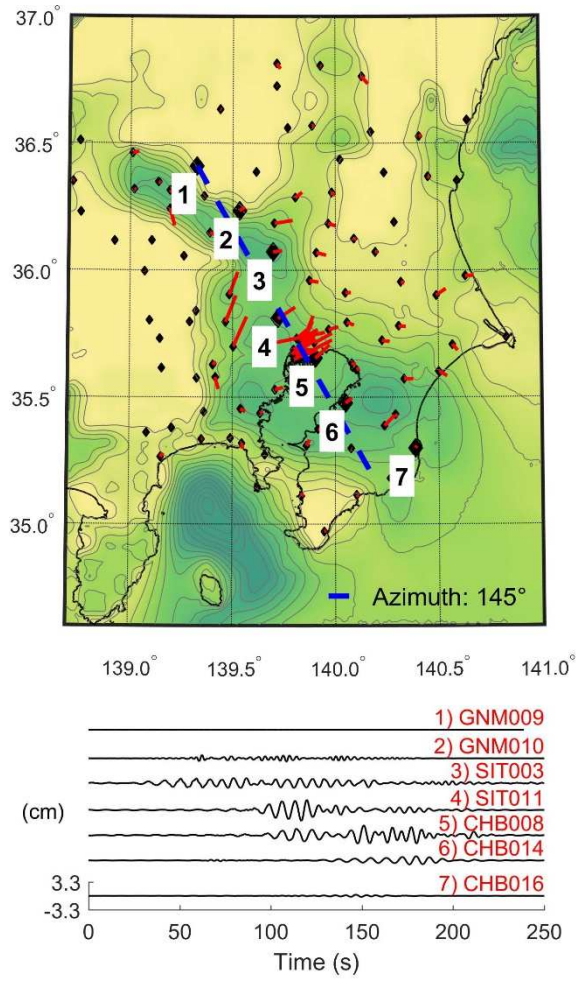


Figure 17. Prograde Rayleigh waves in the Kanto basin extracted in the frequency range 0.1-0.5 Hz. (a) During the Chuetsu earthquake, (b) during the Chuetsu-oki earthquake.

(a)



(b)

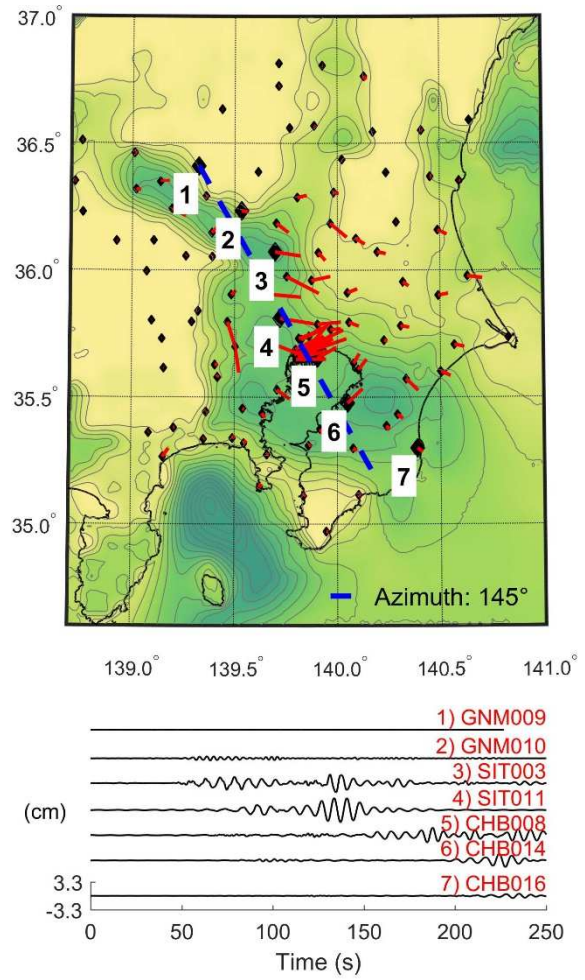


Figure 18. Love waves in the Kanto basin extracted in the frequency range 0.1-0.5 Hz. (a) During the Chuetsu earthquake, (b) during the Chuetsu-oki earthquake.

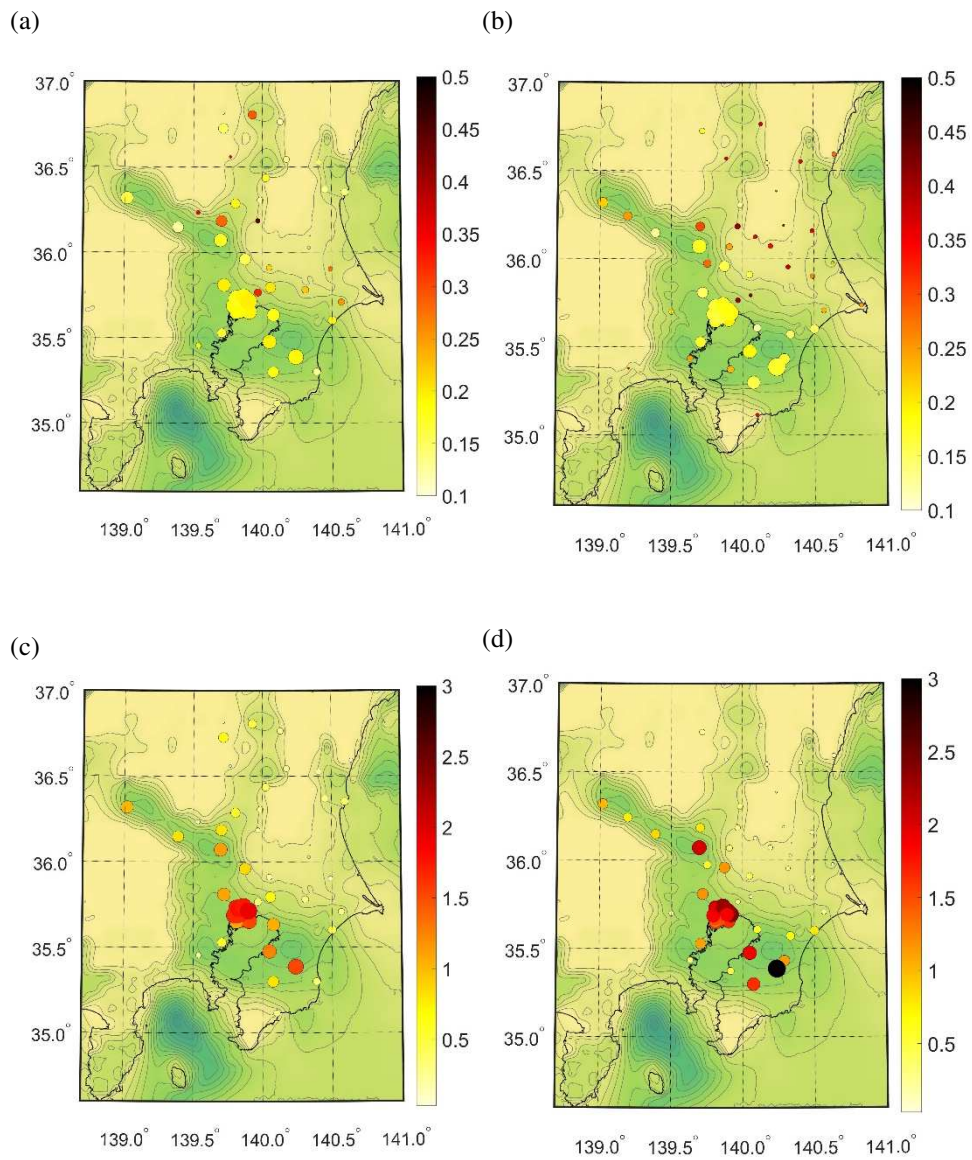


Figure 19. Amplification of prograde Rayleigh waves in the Kanto basin extracted in the frequency range 0.1-0.5 Hz. (a) Central frequency (Hz) during the Chuetsu earthquake, (b) Central frequency (Hz) during the Chuetsu-oki earthquake, (c) Amplification coefficient A_1 during the Chuetsu earthquake, (d) Amplification coefficient A_1 during the Chuetsu-oki earthquake.

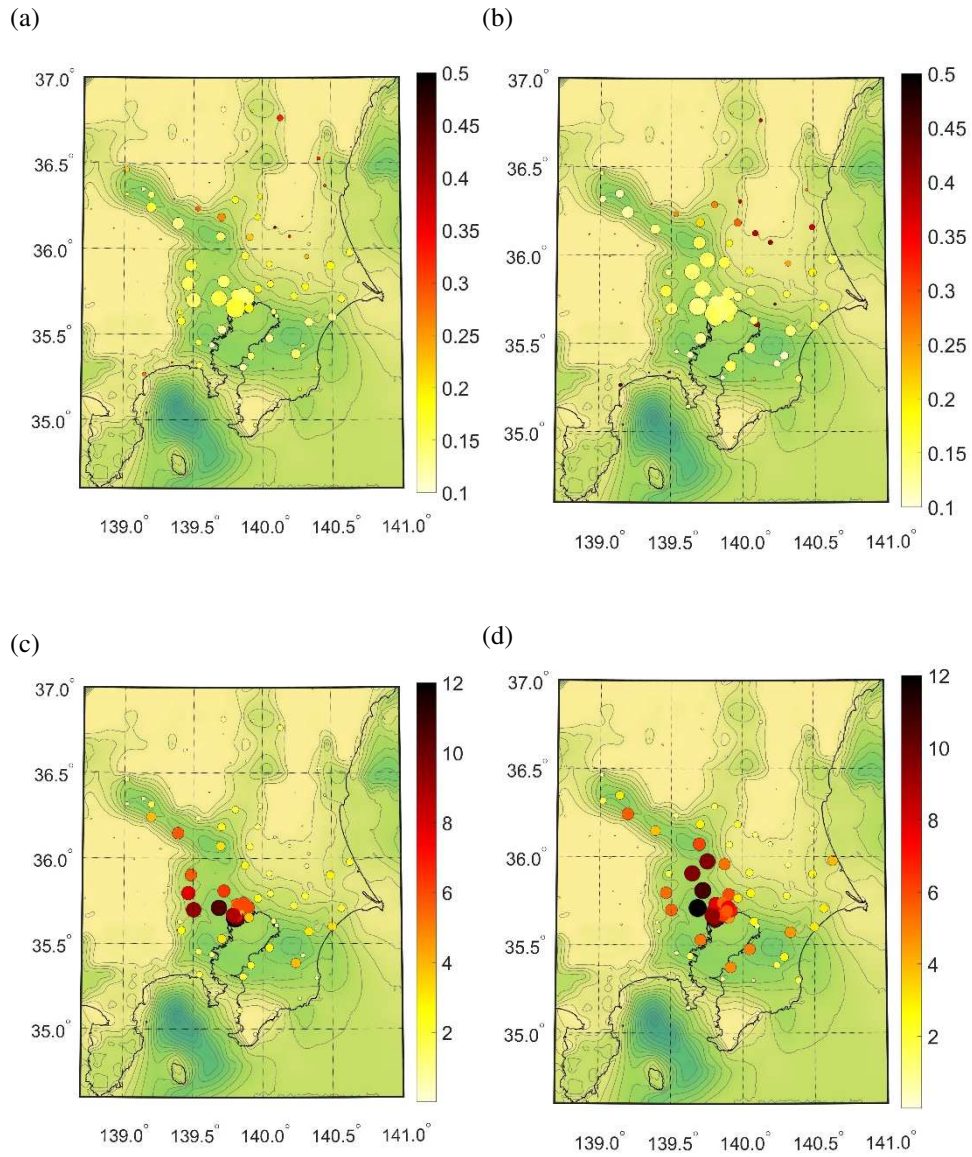


Figure 20. Amplification of Love waves in the Kanto basin extracted in the frequency range 0.1-0.5 Hz. (a) Central frequency (Hz) during the Chuetsu earthquake, (b) Central frequency (Hz) during the Chuetsu-oki earthquake, (c) Amplification coefficient A_1 during the Chuetsu earthquake, (d) Amplification coefficient A_1 during the Chuetsu-oki earthquake.